J. Fluid Mech. (2005), *vol.* 535, *pp.* 287–323.
doi:10.1017/S0022112005004854 Printed in the United Kingdom

Intrusive gravity currents in a stratified ambient: shallow-water theory and numerical results

By MARIUS UNGARISH

Department of Computer Science, Technion, Haifa 32000, Israel

(Received 30 January 2004 and in revised form 10 February 2005)

The intrusion of a fixed volume of fluid which is released from rest and then propagates horizontally at the neutral buoyancy level in a vertically stratified ambient fluid is investigated. The density change is linear, in a restricted layer or over the full depth of the container, and locks of both rectangular and cylindrical shapes are considered. A closed one-layer shallow-water inviscid formulation is used to obtain solutions of the initial-value problem. Similarity solutions for the large-time developed motion and an approximate box model are also presented. The results are corroborated by numerical solutions of the full two-dimensional Navier–Stokes equations and comparisons with previously published experiments. It is shown that the model is a versatile predictive tool which clarifies essential features of the flow field. Accurate insights are provided concerning the governing dimensionless parameters and the major features of the motion. In particular, the theory predicts and explains: (*a*) the fact that the initial propagation is with constant speed for intrusions released from a rectangular lock; (*b*) the effect of the shape of the lock on the motion; (*c*) the spread with time at some power in the developed stage; and (*d*) the sub-critical (compared to the mode 2 linear waves) speed in a full-depth stratified container configuration. The main deficiency of the shallow-water model is that internal gravity waves are not incorporated, but some insight into this effect is provided by the comparisons with the Navier–Stokes simulations and experiments.

1. Introduction

We consider the mainly horizontal motion which develops when a given volume of fluid of constant density is released into a vertically stratified ambient at the level of neutral buoyancy. The typical configuration is sketched in figure 1. We assume that the density of the ambient fluid varies linearly over a layer of finite thickness or over the full depth of the container, and that the Reynolds number, *Re*, of the flow is large. The intrusion under consideration is a special case of flows called gravity currents, and is a well-known phenomenon in natural and industrial systems (Simpson 1997). Previous investigations were concerned with both experimental observation (mainly with salt-water systems) and theoretical interpretations (Wu 1969; Maxworthy 1980, 1983; Faust & Plate 1984; Amen & Maxworthy 1980; de Rooij 1999; Dugan, Warn-Varnas & Piacsek 1976; Manins 1976; Kao 1976). However, important gaps remain in the theoretical understanding and formulation. In particular, no reliable predictive model based on governing equations is available, and there is even some confusion about the scaling of the variables. Wu (1969) suggested a curve-fit description for the nose position x_N vs. t (time), based on a very restricted set of data. Manins (1976) and Kao (1976) developed box models under the assumption that the shape of the

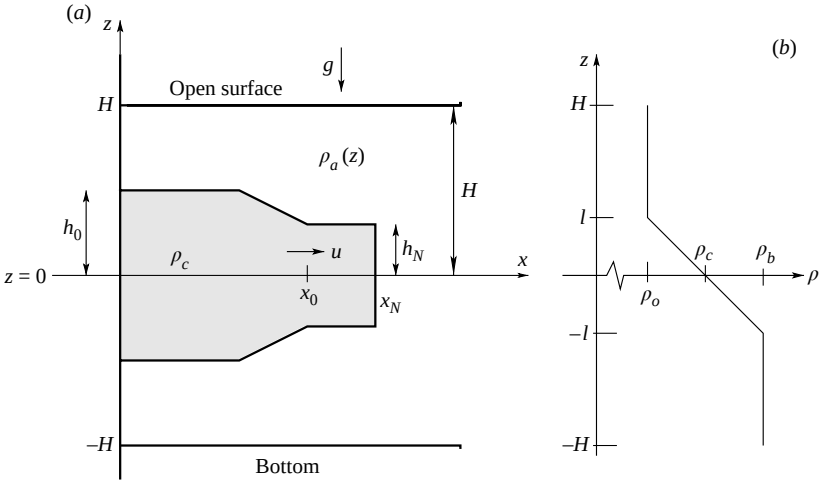

FIGURE 1. Schematic description of the system: (*a*) the geometry after release from a rectangular lock, (*b*) density profile in the ambient. In dimensionless form, the horizontal lengths are scaled with x_0 and the vertical lengths with h_0. The subscripts denote: N – nose (or front); a – ambient; b – bottom; c – current (intrusion); o – open surface.

intruding fluid is an ellipse or a rectangle; both models use adjustable parameters based on some *ad-hoc* matching. Maxworthy (1980, 1983) show that when the thickness $2l$ of the density transition layer is small compared to the thickness of the intrusion, $2h_N$, the solitary-wave description of Benjamin (1967) predicts well the velocity of propagation. This wave problem has a sound theoretical background (for very deep ambients $H/h_N \to \infty$), but is not relevant to the initial stage of propagation of the intruding fluid and, moreover, it requires external knowledge of the amplitude of the wave (i.e. h_N). Consequently, this approach cannot be used as a predictive model for the initial stages of the lock-release and related problems.

There is agreement between the previous investigators that the velocity of propagation of the front in a full-depth linear stratification is given by $\mathscr{F}\mathscr{N}h_N$, where h_N is the (half) thickness of the intrusion, $\mathscr{N}$ the buoyancy frequency, and $\mathscr{F}$ a 'Froude number'. But these studies present various and inconsistent suggestions for the value and functional behaviour of $\mathscr{F}$, and no systematic way of predicting h_N. It is interesting to note that there is ample experimental evidence that an intrusion released from a rectangular lock in various circumstances propagates for a quite long time interval with constant speed (e.g. Faust & Plate 1984; de Rooij 1999), but there is no theory to predict, or explain, such a behaviour. Similarly, there are experimental indications that spread with t (time) at some power (close to 0.5) occurs at a later stage of propagation, but, again, the theoretical details of this behaviour are obscure. A review of the available body of knowledge led to the conclusion stated by Faust & Plate (1984): 'intrusions into a linearly stratified environment behave very differently from theoretical calculations'. The need to close this gap provided the motivation of the work reported in this paper.

The present work introduces a new analysis, based on the shallow-water (SW) equations of motion and is backed by numerical solutions of the Navier–Stokes (NS) problem. The SW model leads to a hyperbolic system for the velocity and thickness of the intrusion as functions of t and x, subject to realistic initial conditions, and uses no adjustable constants. This model predicts some important features of the motion,

in a manner consistent with the available observations, such as: (*a*) propagation with constant velocity in the initial stage for rectangular lock configuration); (*b*) the dependence of the velocity on the thickness of the density-transition layer, $2l$; (*c*) the differences between the flows generated by rectangular and cylindrical locks; (*d*) the 'sub-critical' property of the velocity of propagation; and (*e*) the propagation with $t^{1/2}$ at large times. Comparisons with experiments and NS results are performed and discussed for two configurations: (i) full-depth rectangular lock (or lock exchange) in a stratified tank where the density variation occurs in a layer of thickness $2l$ which is only a portion of the full depth $2H$; (ii) fully linearly stratified tank, with various height ratios of ambient to lock, for both rectangular and cylindrical locks.

The analytical model used here is an extension of the one-layer shallow-water formulation developed by Ungarish & Huppert (2002) for the investigation of gravity currents which propagate at the bottom of a linearly stratified ambient. The theoretical results were in good agreement with the experiments of Maxworthy *et al.* (2002) and with numerical simulations over a wide range of parameters, which gives confidence in the physical acceptability of the underlying assumptions. Indeed, a major simplification is the assumption that the ambient can be considered quiescent for some significant initial period of time. The neglect of the internal waves in the SW formulation was based on the conjecture that for analytical progress it is feasible, perhaps even necessary, to decouple the current and the waves. Useful insights for this approach are provided by the closely related problem of the stratified flow over a fixed obstacle, a topic covered thoroughly in Baines (1995). In analogy with that problem, the gravity current (or intrusion) is a time-dependent deformable 'obstacle', whose shape interacts with the waves it produces in the ambient, and hence the analytical study of the full time-dependent flow field coupled with a time-dependent boundary condition turns out to be a formidable task. The idea was to circumvent the difficulty by attempting the following decoupling: first, solve for the propagation of the gravity current (or intrusion) under the assumption of an unperturbed ambient; next, consider the perturbations produced in an impulsively started flow over an obstacle of prescribed height $h(x,t)$ above the plane $z=0$. The solution of the first problem for bottom gravity currents, Ungarish & Huppert (2002, 2004), demonstrated that the decoupling provides good results for a period of time, until the waves are able to affect the propagation. The analysis of Baines (1995) indicates that the typical wavelength in the perturbed ambient is $2\pi u_N/\mathscr{N}$. The most problematic cases are of sub-critical propagation (with respect to the leading-mode linear wave in the corresponding ambient, see below), but the experimental and numerical results indicate that in any case the first significant interaction between the waves and the nose of the current occurs at some advanced stage of motion (roughly, after a propagation of at least two wavelengths). Until then, the SW predictions are in good agreement with the measurements. We shall show that the intrusions considered in this paper display a similar behaviour, and that the position where the interaction with the waves becomes important can be estimated.

The structure of the paper is as follows. In § 2 the shallow-water equations of motion and the appropriate boundary conditions are developed and discussed. We apply the SW theory and perform comparisons with available experiments and our Navier–Stokes numerical results for the rectangular lock configuration in § 3. The experiments of Faust & Plate are considered first (§ 3.1), and those of Amen & Maxworthy and de Rooij are discussed next (§ 3.2). The cylindrical-lock system is solved and compared with Wu's results in § 4. Finally, in § 5 we present some concluding remarks. In Appendices A–C we present some details of similarity solutions

and box-model approximations, the Navier–Stokes simulator and the processing of the Amen & Maxworthy experimental data.

2. Formulation and shallow-water (SW) approximation

The configuration is sketched in figure 1. We use an $\{x, y, z\}$ Cartesian coordinate system with corresponding $\{u, v, w\}$ velocity components. Gravity acts in the $-z$-direction. We assume that the sidewalls of the container are vertical (x, z)-planes and the gap between them is large (as compared with the thickness of the intrusion, h_0) and hence the inviscid flow does not depend on the coordinate y, and $v \equiv 0$. Symmetry of the initial configuration with respect of the horizontal plane $z = 0$ is assumed, as follows. The ambient fluid is in the domain $-H \leqslant z \leqslant H$, and is stably stratified; the density of the ambient at $z = 0$ is the mean value over the depth, and the density decrease occurs (linearly) either in a part-depth layer $-l \leqslant z \leqslant l$, or over the full depth (i.e. $l = H$), from ρ_b to ρ_o. The initial position of the intrusive current is in the lock $0 \leqslant x \leqslant x_0$, $-h_0 \leqslant z \leqslant h_0$ (assumed rectangular first). The density of the intruding current is equal to that of the ambient at the symmetry plane $z = 0$. In this respect, the fluid of the intrusion can be regarded as the result of mixing the ambient in the lock, and is also referred to as the 'mixed fluid'. This can be expressed as

$$\rho_c = \rho_a(z = 0) = \tfrac{1}{2}(\rho_o + \rho_b) \tag{2.1}$$

where the subscript a denotes the ambient and c, b, o refer to the current (or intrusion, or mixed), bottom and open surface. It is convenient to use ρ_o as the reference density.

We introduce the reduced gravity,

$$g' = \epsilon g, \tag{2.2}$$

where g is the gravitational acceleration and

$$\epsilon = \frac{\rho_c - \rho_o}{\rho_o}, \tag{2.3}$$

is the reduced density difference.

The density in the intruding current and in the ambient can be expressed as

$$\rho_c = \rho_o(1 + \epsilon), \quad \rho_a = \rho_o[1 + \epsilon\sigma(z)], \tag{2.4}$$

where $\sigma(z)$ represents the form (shape) of stratification, a continuous and typically decreasing (allowing for some piecewise-constant regions) function of z. We consider the linear stratification in a layer $\pm l$ about the midplane,

$$\sigma(z) = \begin{cases} 0 & (z \geqslant l) \\ 1 - z/l & (-l \leqslant z \leqslant l) \\ 2 & (z \leqslant -l) \end{cases} \tag{2.5}$$

where $0 < l \leqslant H$. The limits $l = H$ and $l = 0$ represent the full-depth stratification and the two-layer ambient cases, respectively. Extensions of the present analysis to more general forms of $\sigma(z)$ are possible, but the present linear form provides leading-order insight and allows comparisons with available experiments within the simplest mathematical model. The buoyancy frequency is constant and given by (in the density transition layer)

$$\mathcal{N} = \left(\frac{g'}{l}\right)^{1/2} \quad (|z| \leqslant l). \tag{2.6}$$

The following shallow-water approximations are concerned with the inviscid and Boussinesq ($\epsilon \ll 1$) limits. In this case it is justified to claim that, since the initial conditions are symmetric about $z = 0$ (as specified above), the resulting time-dependent flow field will also be symmetric about $z = 0$. It is therefore sufficient to consider the flow in the domain $z \geqslant 0$. (The shape of the density interface and the velocity field in the domain $z \leqslant 0$ are expected to be mirror images.)

We argue that, under the inviscid and Boussinesq assumptions, the $z \geqslant 0$ portion of the intrusion is bound to behave like a gravity current that propagates at the bottom of a stratified tank. This yields a useful connection between the present problem and the recent studies on gravity currents of Maxworthy *et al.* (2002) and Ungarish & Huppert (2002), in particular for the case when the density of the current matches that of the ambient at the bottom (i.e. the parameter called R in Maxworthy *et al.* 2002, and the parameter called S in Ungarish & Huppert 2002 are equal to 1; some care is required in the comparison with these previous formulations, because the top-to-bottom density variation here is larger by a factor 2 compared to the bottom current problems). Compared to the SW formulation of Ungarish & Huppert (2002), not only is the position of the top and bottom boundary changed here, but we consider very different configurations with (*a*) a part-depth density transition layer, and (*b*) cylindrical lock release.

Following these studies, we use a one-layer approximation which is expected to capture many of the important features of the flow, although it discards the internal waves in the ambient, and is the simplest SW model. In the ambient fluid domain we assume that $u = v = w = 0$ and hence the fluid is in purely hydrostatic balance and maintains the initial density $\rho_a(z)$ given by (2.4). The motion is assumed to take place in the intruding layer of fluid only, $0 \leqslant x \leqslant x_N(t)$ and $0 \leqslant z \leqslant h(x, t)$, where the density is ρ_c. The subscript N denotes the nose (front) of the intrusion. We argue that the predominant vertical momentum balance in the intruding fluid is hydrostatic and that viscous effects in the horizontal momentum balance are negligibly small. Hence the motion is governed by the balance between pressure and inertia forces in this horizontal direction. The perturbation of the upper free surface introduced by the flow can be neglected when $\epsilon \ll 1$, as assumed here.

A relationship between the pressure fields and the height $h(x, t)$ can be obtained. In the motionless ambient fluid, which is open to the atmosphere, the pressure does not depend on x, and the hydrostatic balances $\partial p_i/\partial z = -\rho_i g$, where $i = a$ or c, and use of (2.4) yield

$$p_a(z, t) = -\rho_o \left[z + \epsilon \int_0^z \sigma(z')\, \mathrm{d}z' \right] g + C, \tag{2.7}$$

$$p_c(x, z, t) = -\rho_o(1 + \epsilon) g z + f(x, t), \tag{2.8}$$

where the constant C reflects the constant pressure at the top of the ambient at $z = H$. Pressure continuity between the ambient and the intrusion on the interface $z = h(x, t)$ determines the function $f(x, t)$ of (2.8). We obtain

$$p_c(x, z, t) = -\rho_o(1 + \epsilon) g z + \rho_o g' \left[h(x, t) - \int_0^{h(x,t)} \sigma(z)\, \mathrm{d}z \right] + C, \tag{2.9}$$

and consequently

$$\frac{\partial p_c}{\partial x} = \rho_o g' \frac{\partial h}{\partial x} [1 - \sigma(h)]. \tag{2.10}$$

We note in passing that (2.7)–(2.10), although developed for $z > 0$, are also valid in the $z < 0$ domain. Pressure continuity at $z = -h(x,t)$ and $z = h(x,t)$ is equivalent in view of the property $1 - \sigma(h) = \sigma(-h) - 1$, see (2.5).

The fact that $\partial p_c/\partial x$ is not a function of z facilitates the subsequent derivation of the SW equations.

2.1. *Governing SW equations and boundary conditions*

It is convenient to scale the dimensional variables (denoted here by asterisks) as follows:

$$\{x^*, z^*, h^*, l^*, H^*, t^*, u^*, p^*\} = \{x_0 x, h_0 z, h_0 h, h_0 l, h_0 H, Tt, Uu, \rho_o U^2 p\}, \tag{2.11}$$

where

$$T = \frac{x_0}{U}, \qquad U = \left[\frac{\rho_c - \rho_a(z=1)}{\rho_o} h_0 g\right]^{1/2} = (h_0 g')^{1/2} \frac{1}{\mathscr{A}} = \begin{cases} (h_0 g')^{1/2} & (l \leqslant 1) \\ \mathscr{N} h_0 & (l > 1) \end{cases} \tag{2.12}$$

and

$$\mathscr{A} = [1 - \sigma(1)]^{-1/2} = \begin{cases} 1 & (l \leqslant 1) \\ \sqrt{l} & (l > 1) \end{cases} \tag{2.13}$$

(to avoid possible confusion, we specify that ρ_a and σ in (2.12)–(2.13) are calculated at the dimensionless $z = 1$).

Here, again, x_0 and h_0 are the initial length and half-thickness of the intrusion, U is the typical inertial velocity of propagation of the nose and T is a typical time period for longitudinal propagation over a typical distance x_0. The reference velocity accounts for the fact that the effective driving force is provided by the density difference over the vertical dimension of the intrusion. Consequently, the coefficient $\mathscr{A}$ is needed for achieving a unified formulation to the problems of thin ($l < 1$) and thick ($l > 1$) density transition layers (as compared with the thickness of the intrusion). This is relevant to the configurations considered in this paper following available experimental results. The details will become evident during the discussion of the solutions of these cases.

We emphasize that hereafter the variables x, z, u, t, h, H, l, p are in dimensionless form unless stated otherwise. The geometry under consideration imposes $H \geqslant 1$.

The z-average of the horizontal momentum equation, on account of (2.10), and in conjunction with volume continuity, produces a system of equations for $h(x,t)$ and for the averaged longitudinal velocity $u(x,t)$. (Again, viscous terms are neglected under the assumption that the typical Reynolds number, say $Re = Uh_0/\nu$, is very large.) In characteristic form the simplified continuity and momentum equations are

$$\begin{bmatrix} h_t \\ u_t \end{bmatrix} + \begin{bmatrix} u & h \\ \mathscr{A}^2[1 - \sigma(h)] & u \end{bmatrix} \begin{bmatrix} h_x \\ u_x \end{bmatrix} = \begin{bmatrix} 0 \\ 0 \end{bmatrix}. \tag{2.14}$$

For the stratification assumed in this study the eigenvalues of the matrix of coefficients are real and the set of eigenvectors is full, and hence the system (2.14) is hyperbolic. The characteristics propagate with the velocities

$$c_\pm = u \pm \mathscr{A}[h(1 - \sigma(h))]^{1/2}, \tag{2.15}$$

and the relationships on $\mathrm{d}x/\mathrm{d}t = c_\pm$, are

$$\mathscr{A}\left[\frac{1 - \sigma(h)}{h}\right]^{1/2} \mathrm{d}h \pm \mathrm{d}u = 0. \tag{2.16}$$

The initial conditions for the intrusion at $t = 0$ are: zero velocity, unit length and prescribed $h(x)$ (rectangular or cylindrical lock). Boundary conditions at $x = 0, x_N(t)$

are prescribed as follows: $u = 0$ at the backwall $x = 0$, and an additional condition for the velocity u is needed at the nose $x = x_N(t)$ (the values of h at the boundaries follow from (2.15)–(2.16)).

Ungarish & Huppert (2002) argued that, for a bottom gravity current, the velocity of the nose is proportional to the square-root of the pressure head (per unit mass) and, moreover, that the factor of proportionality, defined as the Froude number, Fr, is provided by the same correlation as in the homogeneous gravity current. These arguments are supported by the good agreement between the calculated u_N and the experimental values of Maxworthy *et al.* (2002), and it makes sense to extend them to the present problem, pending the subsequent verification of the results by experiments.

The appropriate pressure head is given by $p_c - p_a$ at $z = 0$ and $x = x_N$, see (2.7) and (2.9), scaled with $g'h_0/\mathscr{A}^2$, and the resulting nose velocity can be expressed as

$$u_N = Fr(h_N)h_N^{1/2}\ [1 - \Lambda(h_N)]^{1/2}\mathscr{A}, \tag{2.17}$$

where

$$\Lambda(h_N) = \frac{1}{h_N}\int_0^{h_N} \sigma(z)\,\mathrm{d}z. \tag{2.18}$$

The term in the square brackets of (2.17) is typically smaller than 1, and expresses the explicit slow-down of the head due to the stratification effects.

To close the formulation, it is necessary to specify the coefficient called the Froude number, Fr. The theoretical formula developed by Benjamin (1968) for homogeneous fluids in idealized situations indicated that this is an increasing function of H/h_N whose maximum is $\sqrt{2}$. The experimental evidence for practical gravity currents confirmed the qualitative behaviour, but suggested some quantitative corrections to account for viscosity and mixing effects. As a semi-empirical compromise, Huppert & Simpson (1980) derived a simple well-known curve-fit-type correlation, which we shall also use here:

$$Fr = \begin{cases} 0.5H^{1/3}h_N^{-1/3} & (0.075 \leqslant h_N/H \leqslant 1) \\ 1.19 & (0 \leqslant h_N/H \leqslant 0.075,\ \text{deep intrusion}). \end{cases} \tag{2.19}$$

This formula contains an empirical adjustment, but we emphasize that this is an accepted 'off-the-shelf' result for gravity currents in general circumstances (e.g. Huppert & Simpson 1980; Bonnecaze, Huppert & Lister 1993; Hallworth, Huppert & Ungarish 2001), not something tailored for the present problem.

No rigorous theoretical derivation of Fr for a stratified ambient configuration is available. Here Fr represents the hindering effect of the ambient fluid on the buoyancy-driven propagation of the nose. We can argue that this effect is dominated by the momentum transport of the displaced fluids, and hence, under the Boussinesq approximation, the stratification of the ambient is expected to have little influence on the dependence of Fr on h_N/H. This justifies the use of a homogeneous-ambient correlation in the present case. This conjecture is supported by the the work of Ungarish & Huppert (2002) which considered the velocities of propagation of a bottom gravity current in a linearly stratified tank. The SW velocities, calculated with the Fr closure (2.19), were in very good agreement with experimental measurements over the full range of the tested parameters. We shall show that this conjecture is also consistent with the configurations discussed in the present work. Moreover, we stress that the subsequent analysis is not affected by the exact form of the closure correlation for $Fr(h_N/H)$. Consequently: (*a*) except for some minor numerical details, the conclusions concerning the main features of the propagation remain valid for a more general

correlation; and (*b*) when an improved theoretical *Fr* is available, its incorporation in the present theory will be a straightforward task.

It is convenient to use the term 'deep' to refer to the case where the ratio h_N/H is so small that *Fr* is practically a constant. For the correlation (2.19) this ratio is simply $0.075 = 1/13.3$. An intrusion may be deep from the start, or become so eventually as a result of its spreading during the propagation. The clear-cut definition of the constant-*Fr* domains, and the simple function in the varying-*Fr* domain are advantages of (2.19).

An inspection of the closed formulation shows that the form of the stratification, i.e. $\sigma(z)$, enters via three effects: (i) the scaling coefficient $\mathscr{A}$; (ii) the pressure gradient in the momentum equation (the coefficient of h_x in (2.14)) and (iii) the nose velocity driving force (the square brackets term in (2.17)). The second effect also affects the propagation of the characteristics. The case of an interfacial intrusion into a two-layer ambient is recovered for $l = 0$, but this case is outside the scope of our investigation (see de Rooij, Linden & Dalziel 1999 where other references are given).

2.2. *Discussion*

The formal assessment of the inviscid SW models, in particular the one-layer approximation, poses a serious challenge even in the classical homogeneous-ambient case. Rigorously, this is an asymptotic theory for a strictly two-dimensional stable flow field in the limits $\epsilon \to 0$, $h_0/x_0 \to 0$, $Re \to \infty$ and $H \to \infty$. In these (sometimes singular) limits, ambiguities concerning the boundary conditions may appear. For obtaining meaningful solutions some rather *ad-hoc* closure conditions are used (for example, *Fr* correlations developed for steady flows are applied to time-dependent fields). There are no stringent theoretical estimates of the errors expected when this theory is applied to real fluids and containers. Consequently, the practical use of this theory is instead based on order-of-magnitude arguments and a confidence-building interaction of comparisons between predictions and observations. In experiments, some deviations from the theoretical assumptions are imposed by various limitations of the equipment (e.g. $\epsilon > 0.01$, $h_0/x_0 > 0.2$, and H is rarely larger than 4) and unavoidable side-effects (e.g. the gate-removal delay, the finite thickness of the shear-mixing zone at the interface between the fluids). Numerical simulations are subject to similar practical restrictions. Consequently, an agreement within several percent between the SW theory and the measurements (or Navier–Stokes results) is the best that can be expected.

In this spirit, we suggest the following main justifications of the present one-layer model. We employ the analogies provided by the homogeneous counterpart and hindsight provided by the solutions discussed below. The return flow in the ambient introduces a relative error $O[(h_N/H)^2]$ to the one-layer simplified pressure term, and hence, since typically $h_N \approx 0.5$, this perturbation may be small even for non-large H. Moreover, the two-layer model (in the homogeneous case) indicates that this perturbation is diminished in regions of small $\partial h/\partial x$, which are typical of the slumping stage in a rectangular lock. On the other hand, the hindering effect of the return flow is accounted for in the correlation of *Fr* as a function of h_N/H which is expected to be correct for all $H \geqslant 1$. All this provides a plausible explanation for the observation that the one- and two-layer models results are in fair agreement concerning the initial propagation even for $H = 1$ (see for example Klemp, Rotunno & Skamarock 1994 and Ungarish & Zemach 2005). The stratified ambient adds the complication of deflected isopycnals and internal waves. However, the hydrostatic approximation for flows over obstacles (see Baines 1995) is consistent with these perturbations in conditions compatible with our problem. The pertinent restriction

to wavelengths larger than $u^*/\mathcal{N}$ (Baines 1995), is, roughly, equivalent to $h_0/x_0 < 1$ in our case. The waves which propagate with the intrusion have, initially, a small amplitude and occupy a relatively small domain. Consequently, the net pressure effect, averaged over time and distance, is expected to be small compared with the main hydrostatic balance. The waves that are radiated ahead in the sub-critical case ($u_N < u_{wave}$) encounter a relatively large volume of ambient fluid and therefore cause very small perturbations (including the columnar mode). Finally, there is evidence (again, mostly for the homogeneous case) that the SW theory, although developed for $h_0/x_0 \ll 1$, reproduces well observations even for h_0/x_0 close to 1. We expected (and to some extent confirmed, in Ungarish & Huppert 2002, 2004 and in the present work) similarly good performances for the SW extensions to the stratified ambient. Since agreements with experimental observations were obtained for a fairly large parameter range (various stratifications, density differences, fractional depths, aspect ratios, lock geometries) without using any adjustable parameter, this cannot be coincidence.

The deeper reason for this agreement seems to be as follows. The real motion of a body of fluid released from rest in an initially hydrostatic ambient looks complicated because of various interfacial effects, but on average the bulk is driven by a simple internal mechanism, which interacts with the external fluid mainly at the front. The SW model contains the z-averaged volume and momentum equation which cast this mechanism into a hyperbolic system with the correct initial and boundary conditions. The information in this fluid is indeed propagated back and forth by the SW waves (characteristics). In this manner, the dynamic behaviour in the interior (including the proper initial potential energy) is matched to the conditions at both the backwall and the front. The front (or shock) condition was derived from a global momentum-integral conservation law and hence for the hyperbolic system picks up the physically meaningful 'weak solution', i.e. the proper velocity of propagation. As the intrusion spreads out, its energy and inertia decay. Eventually, the viscous forces become dominant and invalidate the model. In the stratified sub-critical case (such as considered here) the failure of the model may also occur in the inviscid stage due to a wave–nose interaction, as discussed in § 3.2.

2.3. *Method of solution*

In general, the SW system must be solved numerically. Here we employed a finite-difference two-step Lax–Wendroff scheme (Morton & Mayers 1994; Press *et al.* 1992). This method has been used successfully for non-stratified gravity currents in various circumstances (Bonnecaze *et al.* 1993; Ungarish & Huppert 1998) and here the necessary modifications of the equations and boundary conditions for a symmetric intrusion in a full-depth linearly stratified ambient were made. The domain $0 \leqslant x \leqslant x_N(t)$ was mapped into $0 \leqslant y \leqslant 1$, and the latter discretized into equidistant intervals. In this work we used, typically, a grid with 200 intervals and the time step 0.005. The code was subjected to various validation tests, including repetitions of runs with smaller grid intervals and time steps.

Of particular interest to the present study are the insights provided by the analytical results of the SW equations. A slumping stage and a similarity behaviour can be detected during the initial and advanced phases of motion, respectively. These features are amenable to analytical solutions.

We loosely call 'slumping' the phase after the release during which a dramatic change of shape of the intrusion occurs. Moreover, the SW model predicts that when the release is from a rectangular lock, in this initial stage the intrusion displays a very special feature: the velocity of propagation, u_N, is constant while the intrusion

propagates over a distance of one or more lock lengths (this value of u_N is attained instantaneously in the inviscid model). This prediction of the SW formulation is supported by observations in various experiments as detailed later. The present formulation provides an analytical solution of this constant velocity of propagation via the method of characteristics. Indeed, upon the removal of the vertical gate, the mixed fluid in the rectangular-lock domain is subject to a 'dam-break' type of motion (see also Ungarish 2005). A depression wave of speed $c_- = -\mathscr{A}[1-\sigma(1)]^{1/2}$ propagates from the gate $x=1$ to the backwall $x=0$, and the front (nose) starts to propagate forward as a discontinuity. A shrinking domain of stationary fluid of height 1 exists between the wall and the backward-moving depression wave, and a rectangular domain of fluid of constant height h_N and velocity u_N forms behind the nose. A typical characteristic moving forward with velocity c_+ from the former to the latter domain carries the information $u=0$ and $h=1$. Integration of (2.16) along this characteristic gives u_N as a function of h_N. On the other hand, u_N must satisfy the nose condition (2.17). The intersection of these relationships yields

$$u_N = \Upsilon(1) - \Upsilon(h_N) = Fr(h_N)h_N^{1/2}\ [1-\Lambda(h_N)]^{1/2}\mathscr{A}, \tag{2.20}$$

where

$$\Upsilon(h) = \mathscr{A}\int_0^h \left[\frac{1-\sigma(h')}{h'}\right]^{1/2} \mathrm{d}h'. \tag{2.21}$$

In general, the solution of this nonlinear equation for h_N provides the value of u_N. More explicit forms are obtained for the specific stratifications discussed below.

For release from a cylindrical lock the initial slumping velocity of propagation is not constant. This more complex behaviour, not amenable to a simple analytical solution, will be discussed in § 4.

A similarity solution can be obtained for a deep intrusion after the initial conditions are 'forgotten'. We shall show in Appendix A that in this case $x_N(t) \sim t^{1/2}$, while u and h are simple functions of $y = x/x_N(t)$. We recall that the similarity solution of a deep gravity current in a homogeneous ambient displays the notably different $x_N(t) \sim t^{2/3}$ and also a different shape of $h(y)$ (see Grundy & Rottman 1985, where other pertinent references are given).

Quantitative results and comparisons are discussed below for typical configurations (two with rectangular locks, one with a cylindrical lock).

3. Rectangular lock configurations

3.1. *Part-depth transition layer and full-depth lock*

Here we consider the cases with fixed $H=1$ and various l. This configuration corresponds to the laboratory investigation of Faust & Plate (1984). The intruding (mixed) fluid initially occupies the full depth of the tank, and the ambient is composed of a lower layer of 'heavy' fluid, an upper layer of 'light' fluid, and a linear transition layer (see figure 1). In this case $\mathscr{A}=1$, i.e. the reference velocity is $U=(g'h_0)^{1/2}$.

The relevant experiments were performed with salt water (clearly in the Boussinesq range) in a tank of 300, 50 and 20 cm length, depth and width. Intrusions with $Re \gg 1$ produced by various combinations of fluid depth (h_0), lock length (x_0), thickness of density transition layer (l) and total density variation (ϵ) were tested. The major qualitative observation was that, in all experiments, the nose of the intrusion propagated with constant velocity for a relatively long distance (practically, over all the measured interval). The major quantitative result is the value of this velocity of

propagation. Indeed, the ratio of this measured constant velocity to $2(g'h_0)^{1/2}$ (V_* in the notation of that paper) is displayed in figure 7 of Faust & Plate (1984), and provides a very reliable and convenient set of data for direct comparison with the values of $0.5u_N$ predicted by our theory.

The present SW theory predicts propagation with constant velocity during the initial slumping phase. This prediction is indeed in full agreement with the observations. The theoretical value of the slumping velocity u_N is provided by (2.20)–(2.21). Let us be more specific. Here $l \leqslant H = 1$, and therefore

$$\Upsilon(1) = \int_0^l \frac{1}{l^{1/2}}\,\mathrm{d}h + \int_l^1 \frac{1}{h^{1/2}}\,\mathrm{d}h = 2 - l^{1/2}. \tag{3.1}$$

To proceed, we must distinguish between the following possibilities:

1. Thin density transition layer, $l < h_N$. The calculation of $\Upsilon(h_N)$ and $\Lambda(h_N)$, see (2.21) and (2.18), use of (3.1) and substitution in (2.20) yield

$$u_N = 2\left(1 - h_N^{1/2}\right) = Fr\, h_N^{1/2}\left(1 - \frac{1}{2}\frac{l}{h_N}\right)^{1/2}. \tag{3.2}$$

The largest u_N is expected for $l = 0$, i.e. the two-layer fluid limit.

2. Thick transition layer, $l > h_N$. Similar calculations give

$$u_N = 2 - l^{1/2} - \frac{h_N}{l^{1/2}} = \frac{Fr}{(2l)^{1/2}} h_N. \tag{3.3}$$

Here the simplest case is the $l = 1$ limit for which the minimal u_N is expected.

The function $u_N(l)$ is continuous at $l = h_N$ where a switch from (3.2) to (3.3) occurs. The right-hand sides of (3.2)–(3.3) predict a remarkable reduction of velocity from $l = 0$ to $l = 1$: owing to the stratification the velocity of propagation becomes proportional to h_N (instead of $h_N^{1/2}$) and is further reduced by $\sqrt{2}$ (Fr changes little in this case).

Since $H = 1$, Fr is a function of h_N only. The only free variable in (3.2)–(3.3) is l. Consequently, the present SW theory predicts that the velocity of the intrusion, scaled with $U = (g'h_0)^{1/2}$, is a function of the thickness of the density transition layer, scaled with the initial thickness of the intrusion. This prediction is, again, in full agreement with the experimental results of Faust & Plate (1984).

A quantitative comparison is performed next and displayed in figure 2. Both experiment and theory show a monotonic and quite strong decrease of velocity with l. The SW results are equal to or slightly below the experimental values (typically by about 5 %, the experimental error is about 4 %). We think that the agreement between theory and experiments can be considered as very good, in view of the idealizations used in the model. Indeed, the typical density difference ϵ in the experiment was 3 %, and hence the errors associated with the Boussinesq simplification are already of the magnitude of the discrepancy.

To summarize: we think that the good agreement of the analytical results, over the full range of l, with the experiments of Faust & Plate (1984) provides strong support for our SW theory. We notice that the attempts of Faust & Plate (1984) to interpret their results in the framework of previous theories failed, and led the authors to the conclusion (p. 325) "intrusions into a linearly stratified environment behave very differently from theoretical calculations". In this context, significant progress has been achieved: our SW theoretical results predict well the real propagation of an intrusion as measured by Faust & Plate (1984).

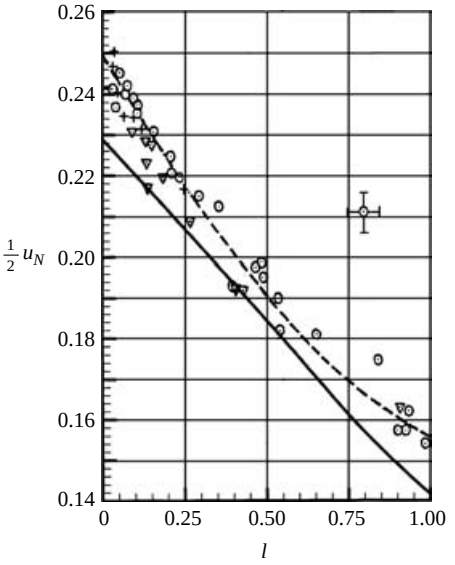

FIGURE 2. Comparison with figure 7 of Faust & Plate (1984): $0.5u_N$ (defined as F_D in that paper) as a function of l. The solid line is the present SW prediction, the points and dashed line are the experimental measurements and the corresponding curve-fit from Faust & Plate (the cross bars show the experimental error).

3.2. *Fully linearly stratified tank, part-depth locks*

Here we consider cases with $l = H$ and various H. This configuration corresponds to the laboratory investigations of Amen & Maxworthy (1980) and de Rooij (1999). The coefficient $\mathscr{A} = \sqrt{H}$, see (2.12)–(2.13), and hence the reference velocity and time can be expressed as

$$U = \left(\frac{g'h_0}{H}\right)^{1/2} = \mathscr{N}h_0, \quad T = \mathscr{N}^{-1}\frac{x_0}{h_0}. \tag{3.4}$$

The dominant waves in the stratified ambient, symmetric about $z = 0$, are the linear mode 2 waves (see Baines 1995 and Amen & Maxworthy 1980), and their (dimensionless) speed is

$$u_{wave} = \frac{1}{\pi}H. \tag{3.5}$$

Substitution of $l = H$ and $\mathscr{A} = \sqrt{H}$ renders the equations of motion (2.14) as

$$h_t + (uh)_x = 0, \tag{3.6}$$

$$u_t + \tfrac{1}{2}(h^2)_x + \tfrac{1}{2}(u^2)_x = 0, \tag{3.7}$$

the nose velocity condition (2.17) as

$$\frac{\mathrm{d}x_N}{\mathrm{d}t} = u_N = Fr\frac{1}{\sqrt{2}}h_N, \tag{3.8}$$

and the characteristic balances (2.15)–(2.16) as

$$\mathrm{d}h \pm \mathrm{d}u = 0 \quad \text{on} \quad \frac{\mathrm{d}x}{\mathrm{d}t} = c_\pm = u \pm h. \tag{3.9}$$

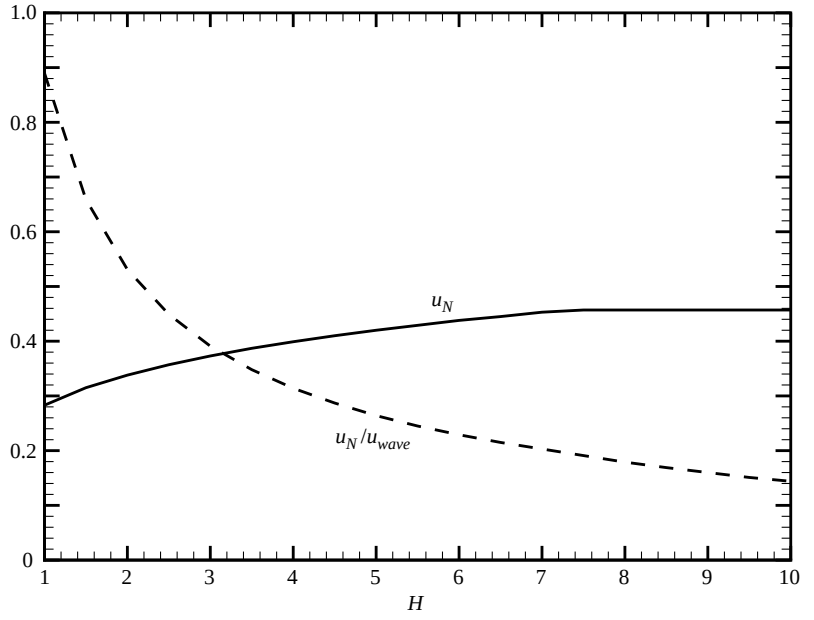

FIGURE 3. Slumping stage u_N and u_N/u_{wave} as a functions of H in rectangular lock release.

In this case the first and very significant phase is, again, propagation with constant velocity provided by the 'slumping' result. Substitution of $l = H$ in (2.5) and subsequent use of (2.20) yield the slumping velocity

$$u_N = (1 - h_N) = \frac{Fr}{\sqrt{2}} h_N. \tag{3.10}$$

The influence of H enters via Fr, which is expected to increase with H, but not dramatically. The behaviour of u_N as a function of H is shown in figure 3. The small variation (from 0.28 to 0.46) over the entire range of H confirms the choice of the scaling quantities. Also shown in this figure is the velocity ratio between the intrusion and the dominant wave, see (3.5). This ratio is smaller than 1 for $H = 1$ and decreases as H increases; in other words, the nose velocity is always sub-critical. This prediction is consistent with the available experiments.

Typical results are discussed below.

(i) *Comparisons for* $H = 1$

This case (full-depth or lock-exchange release) is of particular interest because it is, apparently, the simplest and hence the most attractive, from the experimental point of view. It is also the meeting point of the investigations of Faust & Plate (1984), Amen & Maxworthy (1980) and de Rooij (1999). On the other hand, this is the most problematic case from the point of view of the SW theory, because of the strong return flow in the ambient above and below the intrusion. The one-layer SW model used here (that assumes a motionless ambient) is expected to lose accuracy. However, the formal deviations from the one-layer assumptions, caused by the return flow, are not so severe and even compensated, as explained in § 2.2. Indeed, as shown below, the model still provides useful and accurate predictions.

In the SW scaling this case has no free parameters, and the slumping velocity is $u_N = 0.283$ (for the Fr correlation used here). We can make a straightforward

comparison with the experiments of de Rooij (1999), performed with a saline solution, a lock of $h_0 = 0.5x_0 = 10\,\mathrm{cm}$ in tanks of various lengths ($\leqslant 100\,\mathrm{cm}$) and $\mathscr{N} = 1.0\ \mathrm{s}^{-1}$ (the assumptions of Boussinesq and inviscid fluid were satisfied well). In all cases, the velocity of propagation remained constant over at least 5 lock lengths and its value was $2.9\,\mathrm{cm\,s}^{-1}$ which, in our scaling, is equal to 0.29. Again, the agreement with the SW theory is excellent. As in the part-depth density transition layer case, the measured velocity of propagation is larger than the SW prediction, but the discrepancy of 2 % only is certainly remarkable.

Two experiments of Amen & Maxworthy (1980), namely runs 167 and 170 listed in table 1 of that paper, are also with $H = 1$, but the reported propagation is about ten times faster than that obtained in other compatible configurations (e.g. Faust & Plate 1984 for $l = 1$ and de Rooij 1999). We therefore think that these discrepancies must be attributed to a misprint; as suggested by Faust & Plate (1984), it would make sense to multiply the printed times by 10. This correction is used hereafter, and good agreement with other experiments and the theory is obtained.†

The relevant NS computation was performed for $H = 1$ and $h_0/x_0 = 1$, to simulate experiments runs 167 and 170 of Amen & Maxworthy (1980), and with $h_0/x_0 = 0.5$ to simulate Ex. 28, 30, 38, 40 of de Rooij (1999). In the computations the tank was of length $x_\mathrm{w} = 5$ and the grid had 280×160 intervals. The wave propagating into the unperturbed ambient with $u_{wave} = 1/\pi$ did not reach wall at x_w during the time interval considered here. The main difference between these runs is the value of h_0/x_0. (Following the experimental data, in the simulations for Amen & Maxworthy we used $Re = 6.7 \times 10^4$, see Appendix B, and $\epsilon = 0.0125$, and in the simulation for de Rooij we used $Re = 4 \times 10^4$ and $\epsilon = 0.0100$. Actually, these differences in the small parameters ϵ and $1/Re$ are insignificant.) Various tests were applied to the numerically generated data to confirm their convergence and accuracy. In particular, we compared simulations with different grids, time steps, length of tank, x_w, and various values of ϵ.

Results for the distance of propagation as a function of time are shown in figure 4. There is fair agreement between the results. The NS computations show an initial adjustment delay, but afterwards the velocity of propagation is fairly constant and in agreement with the SW and experimental results, in particular with those of de Rooij. The NS computations confirm the SW prediction that the lock aspect ratio, h_0/x_0, has no influence on the initial velocity of propagation (the details of the short initial velocity nose-adjustment stage are neglected in the inviscid SW theory). According to both SW and NS predictions, the same initial velocity of propagation is expected in the experiments of Amen & Maxworthy and of de Rooij considered here. We notice a scatter of about 12 % between the experimental velocity results of de Rooij and Amen & Maxworthy. The theoretical result is within this uncertainty margin, closer to the measurements of de Rooij. These results show very good agreement between the SW theory and experimental data. (The data of de Rooij 1999 were obtained by repeating experiments and may therefore be considered to provide more accurate results than those of Amen & Maxworthy.)

The SW-predicted propagation is the first to decelerate (after $t \approx 4$). This is a consequence of the one-layer model simplification, which underpredicts the slumping interval when H is close to 1, like in the present configuration. In other words, for configurations with H close to 1 the SW model predicts very well the initial velocity

† We asked the opinion of Professor Maxworthy. He kindly informed us that he did not keep the original records of the experiments, but the suggested misprint correction makes sense.

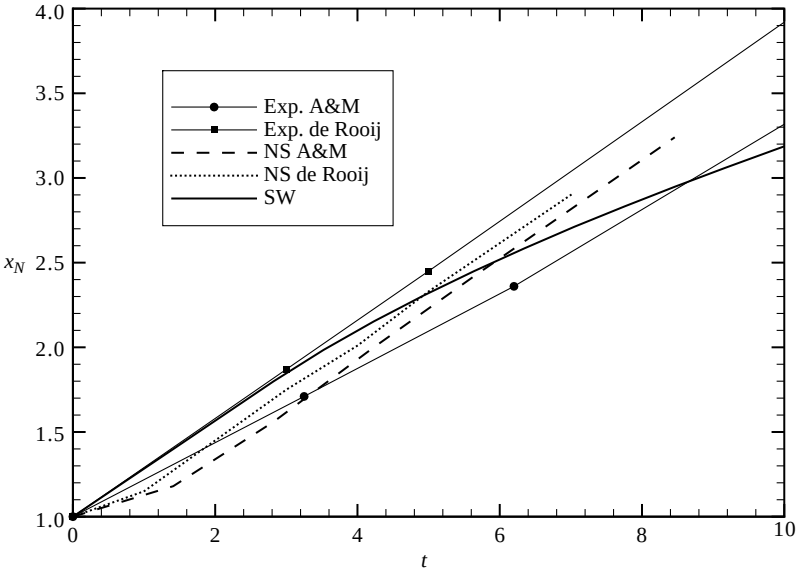

FIGURE 4. Distance of propagation as a function of time for configurations with $H = 1$: results of experiments of Amen & Maxworthy, denoted A & M (with $h_0/x_0 = 1$) and of de Rooij (with $h_0/x_0 = 0.5$); the corresponding NS simulations; and the SW model.

of propagation, but underpredicts the time (or distance) over which the constant velocity stage is maintained. This deficiency of the one-layer model has also been noted for homogeneous currents (Ungarish & Zemach 2005) and is clearly not a problem introduced by the stratification in the ambient.

Density contours of the NS solution are shown in figure 5. The nose of the intrusion is indicated by the $\rangle$ (this is the foremost position of the domain with scaled density $\phi = 0.5$; the contours 0.51 and 0.49 enclose this domain). The NS simulations, performed for the full domain $-H \leqslant z \leqslant H$ as detailed in Appendix B, confirm the SW assumption of symmetry about $z = 0$. Some small deviations appear near the boundaries because in the NS simulations free-slip and no-slip conditions are applied at the top and bottom, respectively, to reproduce a real experimental tank. A numerical test with slip bottom conditions confirmed that this has a negligible effect on the propagation of the intrusion. The resulting shape of the intrusion is in good agreement with the experimental visualizations presented by de Rooij (1999) (figure 5.7). A propagation of the density perturbation ahead of the nose is observed. However, the density perturbations induced by the leading wave are small, at least during the time considered here. This is, again, consistent with the observations of de Rooij (1999). The behaviour of the velocity field is illustrated by contour lines of u in figure 6. The maximum velocity is at the nose and its value is in agreement with the predictions of the SW theory. A quite strong return flow develops between the boundaries and the head of the intrusion, as expected for a shallow ambient (in particular for H close to 1). The flow in the ambient is strongly z-dependent.

The interface of the intrusion is quite smooth at $t = 2.8$ and 4.2, but at $t = 7.1$ some wiggles are observed which reflect the influence of the internal oscillations in the ambient. In spite of these complicated details, the averaged SW formulation is able to predict with fair accuracy the propagation as a function of time. This indicates that, on time and space average, the leading balances are still captured well

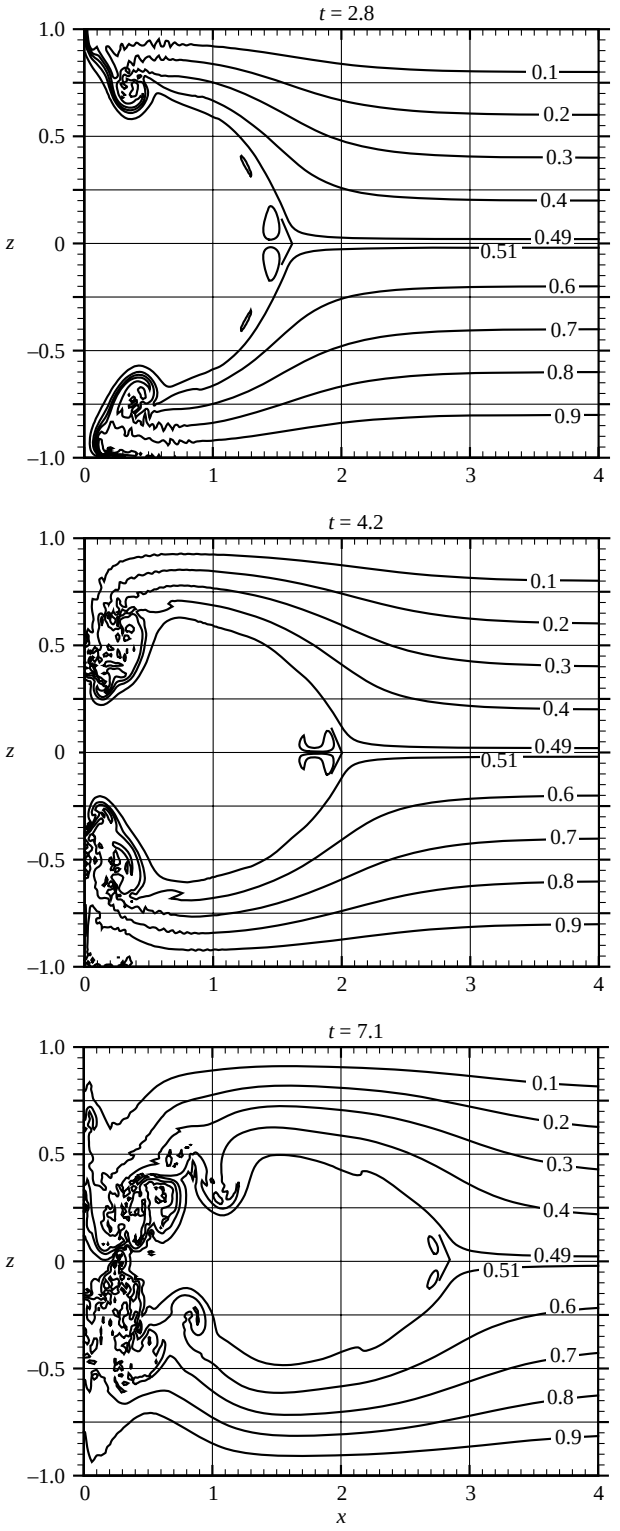

FIGURE 5. Density contour lines for $H = 1, h_0/x_0 = 1$ at various times. NS computations for experiment run 167 of Amen and Maxworthy. The nose is marked by ⟩.

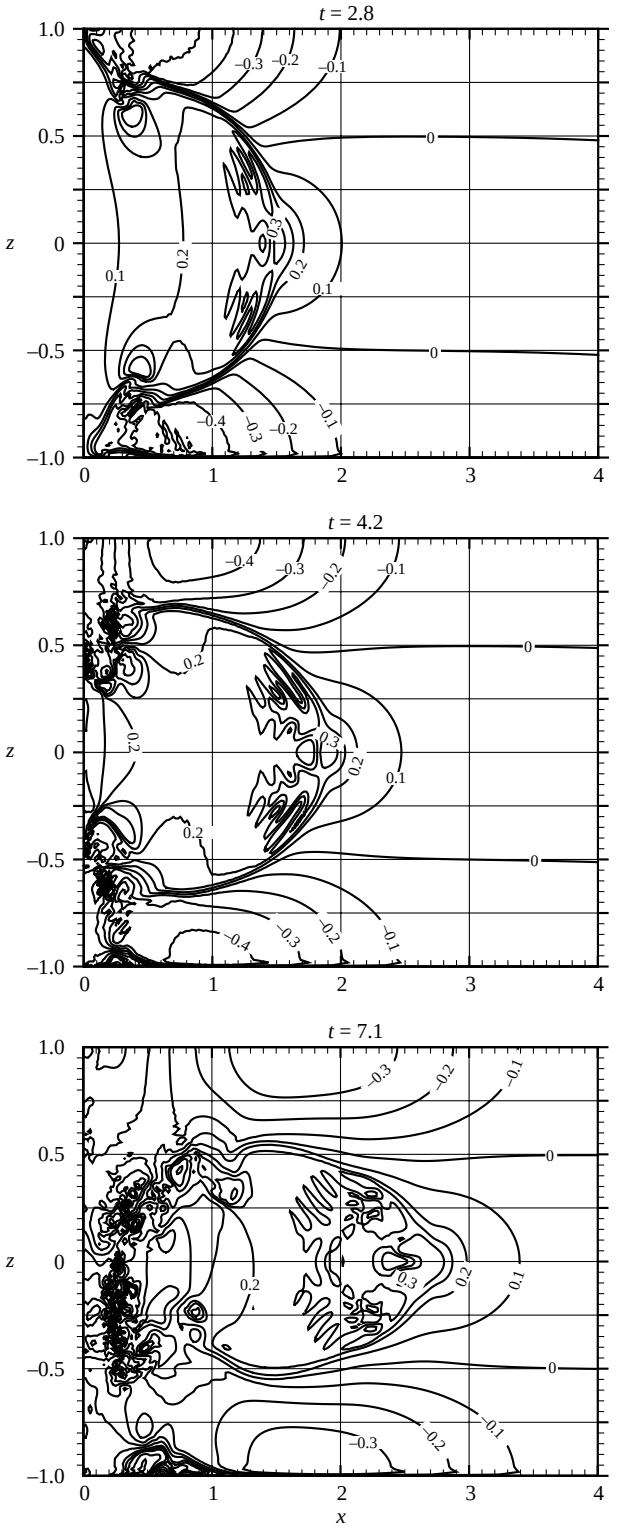

FIGURE 6. u velocity contour lines for $H = 1, h_0/x_0 = 1$ at various times. NS computations for experiment run 167 of Amen and Maxworthy.

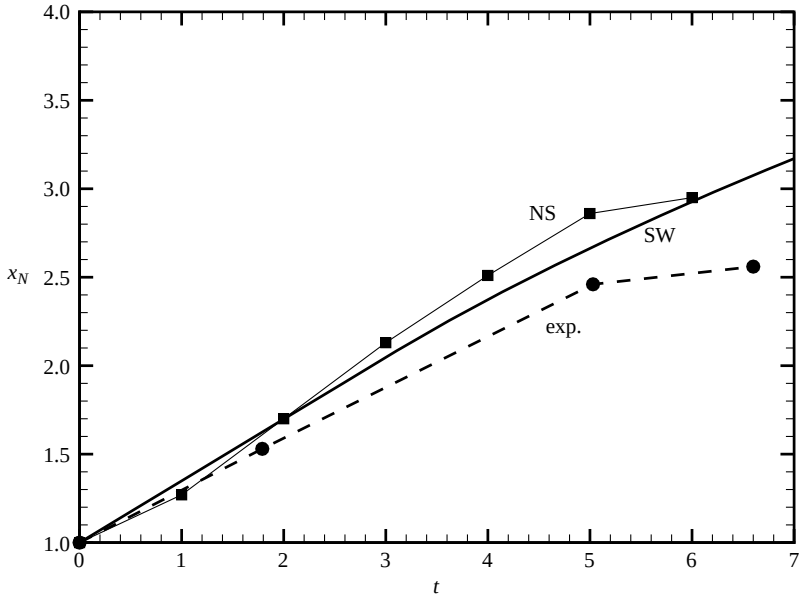

FIGURE 7. Distance of propagation as a function of time for $H = 2.27$: experiment run 117 of Amen & Maxworthy, NS computations, and SW model.

by the shallow-water assumptions, including the Froude condition at the nose, for quite significant length and time intervals. Eventually, the wave–nose interaction may become dominant, but this effect is beyond the range of this simulation, as discussed later.

(ii) *Comparisons for* $H = 2.27$

The experimental points were taken from Amen & Maxworthy (1980), run 117 (salt water, $h_0 = 6.16$ cm, $\mathscr{N} = 0.57$ s^{-1}). The aspect ratio of the lock is $h_0/x_0 = 0.33$, among the smallest in the set of experiments.

The Navier–Stokes solver simulated this configuration using a 260×180 mesh (the numerical tank was of length $x_w = 5.5$), $\epsilon = 4.64 \times 10^{-3}$ and $Re = 2.5 \times 10^4$.

Distance of propagation as a function of time is displayed in figure 7. The experimental and theoretical results are, again, in good agreement. At $t \approx 6$ a strong deceleration of the intrusion is observed in both experiment and NS simulation. This is attributed to the wave–head interaction, discussed later, an effect not resolved by the SW formulation. Indeed, the SW predictions are in very good agreement with the NS computations until this time when interaction begins. In this case the layer of ambient is quite thick compared to that of the intrusion (the typical H/h_N is about 5) and hence the one-layer SW model is expected to be a good approximation.

Consider the density contours of the NS solution shown in figure 8, which reveal the complex wavy features of the flow field. The waves in this case are significantly more pronounced than in figure 5. The main reason is the different value of h_0/x_0 (which is 0.33 in figure 8 and was 1 in figure 5; we estimated that the typical wavelength is $2\pi u_N(h_0/x_0)$. To strengthen this argument, we computed the flow of a configuration similar to that of figure 8, but with $h_0/x_0 = 1$. The results (not displayed here) confirmed that a similar propagation of the intrusion occurs, but with considerably smoother isopycnals (longer wavelengths). Another reason for the wavy appearance

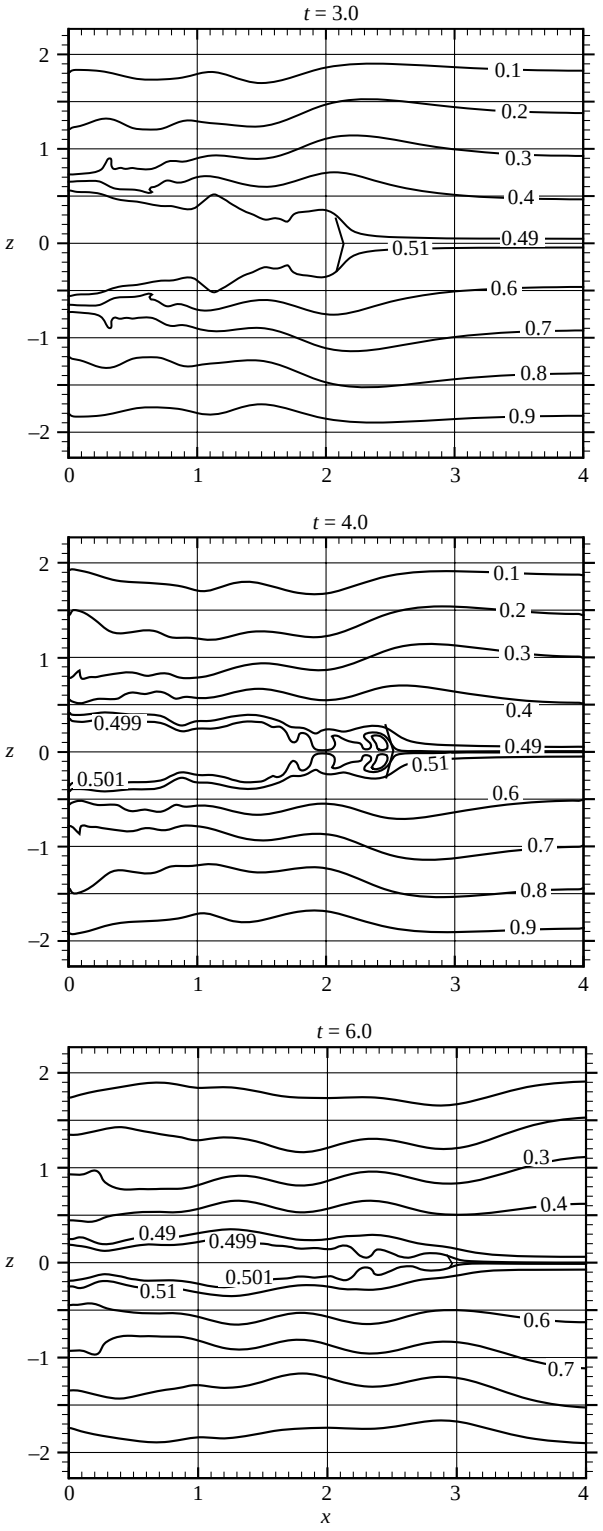

FIGURE 8. Density contour lines at various times, NS computations, for configuration with $H = 2.27, h_0/x_0 = 0.33$ (simulation of run 117 of Amen & Maxworthy). The nose is marked by ⟩.

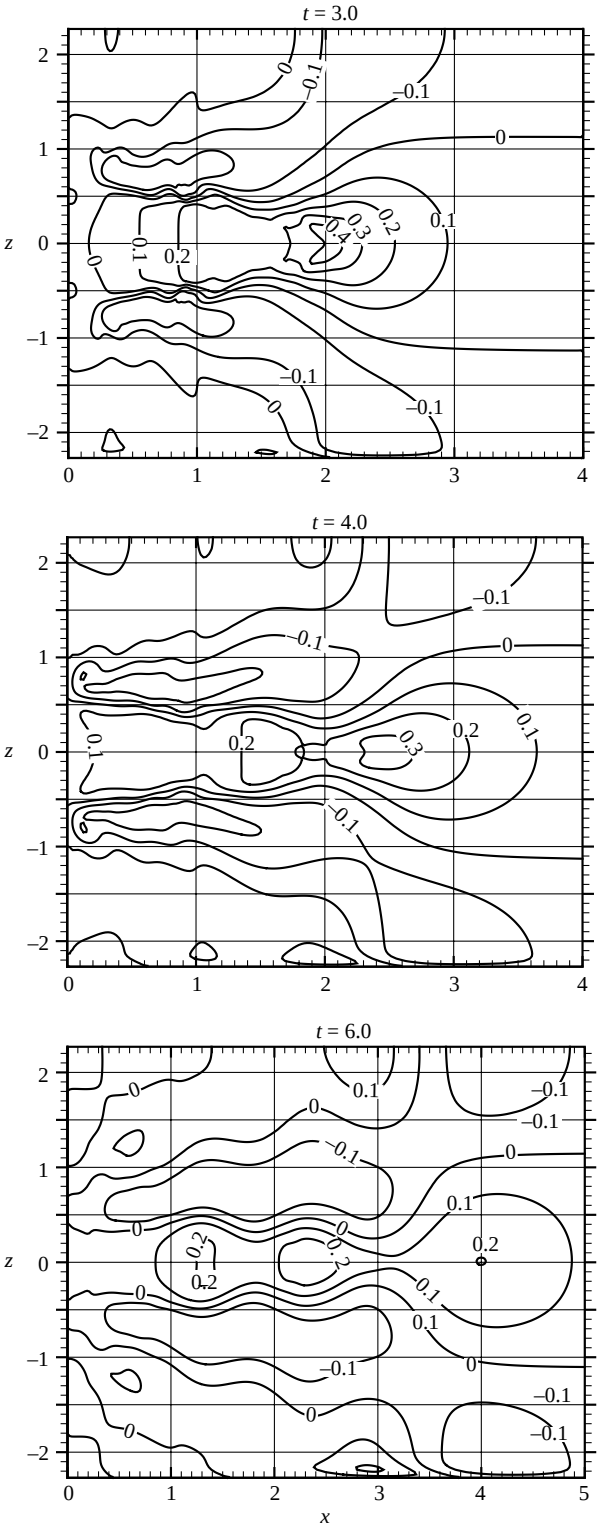

FIGURE 9. u contour lines at various times, NS computations, for configuration with $H = 2.27$, $h_0/x_0 = 0.33$ (simulation of run 117 of Amen & Maxworthy).

of the flow field is the velocity of propagation of the leading waves, see (3.5). In the present configuration $u_{wave} = 0.72$, in contrast to only 0.32 in the case of runs 170 and 167 (figure 5). However, these waves introduce only weak disturbances in front of the intrusion and the length of the tank in the computation was sufficiently large to avoid reflections during the time interval considered.

The velocity field is illustrated by contour lines of u in figure 9. The return flow in the ambient is quite complex and concentrated in layers (or patches) close to the intrusion. At $t = 6$ the nose of the intrusion is at $x \approx 3$, and we observe that the velocity field in this region is quite weak and smeared. This reproduces the effect of the interaction between the waves and the head.

(iii) *A general comparison with the experiments of Amen & Maxworthy (1980)*

The experiments are for $1 \leqslant H \leqslant 2.5$, $0.29 \leqslant h_0/x_0 \leqslant 1.05$, and typical Reynolds number 10^4. In general, our predictions are consistent with the data. However, we also found some exceptions, and our conclusions are based on a selected sub-set. We discarded some experiments which we judged to be inconclusive because of big scatter about the main trend. The details and justifications are presented in Appendix C.

In any case, our interpretation of the data concerning the propagation of the intrusion is different from that of Amen & Maxworthy. Following Wu (1969), Amen & Maxworthy plotted the measured x_N as a function of $\mathcal{N}t^*$ on log-log axes, and marked two special points: (i) the 'lower tangent point' (let us denote its time and position as (t_1, x_1) and (ii) the 'upper tangent point' where a sharp deceleration starts, denoted here (t_2, x_2). Inspired by the observations of Wu (obtained for a cylindrical lock in a quite deep intrusion) they identified the motion from the initial point (0, 1) to (t_1, x_1) as the 'initial collapse stage' and the motion from (t_1, x_1) to (t_2, x_2) as the 'principal stage'. To the later stage Amen & Maxworthy fitted the self-similar form of propagation $x_N \sim t^n$. The values of the tangent points and of the resulting n for 25 experiments are given in table 1 of that paper. The deceleration after t_2 was attributed to viscous effects. There are several objections to this interpretation.

The present SW theory indicates that the rectangular-lock problem of Amen & Maxworthy is expected to be quite different from that of Wu. The stage of self-similar propagation $\sim t^n$ is expected to develop at larger t (compared to Wu), after a slumping stage of constant u_N. An inspection of the results of Amen & Maxworthy indicates that the typical values of x_1 are not sufficiently large for the start of the self-similar phase, and the values of Re at x_2 are not sufficiently small for the start of the dominant viscous influence. Moreover, the experiments of Faust & Plate (1984), de Rooij (1999), and Maxworthy *et al.* (2002) clearly indicate that for release from a rectangular lock the initial propagation is with constant velocity for times and distances similar to the recorded t_2 and x_2. Thus, in order to reconcile the experiments of Amen & Maxworthy with later experiments and with the present theory, a novel interpretation is needed.

Our conjecture is that the results of Amen & Maxworthy up to t_2 can also be fitted into the constant-slumping-velocity framework. This was tested by the calculation of velocities from the data (see Appendix C for details). Nine of the 25 experiments confirm this constant-velocity expectation within about 2 % error, and nine more within about 10 %. We think that this is the correct conclusion from the experimental data. (In the other seven cases the deviation from the constant-velocity pattern is larger, up to about 35 %, but the velocity results are scattered and sometimes lack internal consistency. We therefore think that these results are rather inconclusive and can be discarded from the discussion of the velocity pattern.)

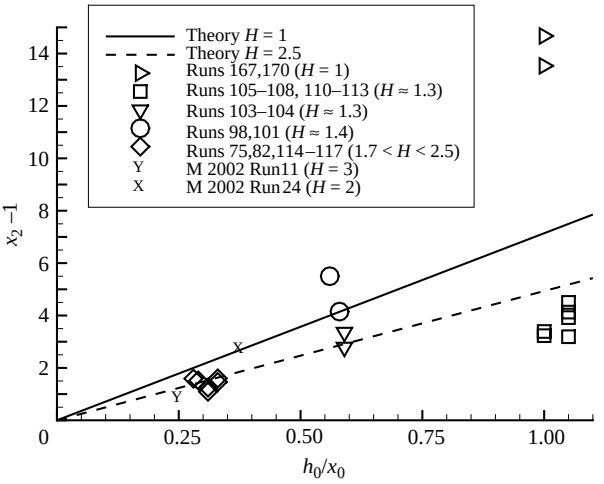

FIGURE 10. Distance of propagation where sharp deceleration begins. The lines are the present estimate of first interaction between waves and nose. The symbols show experiments of Amen & Maxworthy, the X and Y show experiments of Maxworthy *et al.* (2002) (M2002) with bottom gravity currents.

In our interpretation, x_2 is the end of the constant-velocity phase (not the start of the viscous influence). In particular, this may be the point where the first wave–nose interaction occurs (figures 5(*c*) and 5(*e*) of Amen & Maxworthy (1980) indeed display a typical wavy kink at this position). We can estimate theoretically this position as follows. Maxworthy *et al.* (2002) observed that the first wave moves with the head of the current, and after the second wave is created the first wave starts to move relative to the head and affects the velocity when its crest catches the nose. We postulate that this is the generic pattern of behaviour in the time interval from release to interaction. The expected wavelength, scaled with x_0, is $2\pi u_N(h_0/x_0)$ ($2\pi u_N^*/\mathcal{N}$ in dimensional form). Thus, the distance required for the formation of two waves between the position of the gate $x = 1$, and the front $x = x_N$, plus the additional propagation of the wave crest with relative velocity $u_{wave} - u_N$ over the (1/4) wavelength (to the position where maximum interaction is attained), yields

$$x_2 = 1 + 2\pi \frac{h_0}{x_0} u_N \left[2 + \frac{0.25 u_N}{u_{wave} - u_N} \right]. \tag{3.11}$$

Using the values of u_{wave} and u_N provided by (3.5) and (3.10), we find that for a fixed H the resulting x_2 is a linear function of the lock aspect ratio h_0/x_0, and the slope of the line decreases when H increases. Since the return flow in the ambient will reduce the absolute velocity of the wave, our formula is expected to underestimate x_2. Figure 10 shows experimental values of $x_2 - 1$ and the above estimate (for two values of H which bound the experiments of Amen & Maxworthy (1980)). The data of 20 out of 25 experiments seem to collapse in the predicted manner. (The other experimental results displayed values of x_2 larger by more than 100 % than estimated by (3.11), and were not shown. We think that the reason is that the first wave–nose interaction was weak, and therefore not recorded.) To strengthen our conjecture we also added two points from the experiments of Maxworthy *et al.* (2002) (Runs 11 and 24, see table 1 of that paper). These experiments were for bottom gravity currents under

conditions which approximate well a symmetric intrusion, and, again, motion with constant velocity was observed in all cases for a significant distance.

When H is close to 1 the difference between u_{wave} and u_N is small, see figure 3, and therefore the interaction is delayed; this is consistent with the observations. Moreover, in this case the return flow in the ambient is significant, and therefore the real x_2 is significantly larger than our one-layer model estimate, as expected. These considerations explain why the interval of constant velocity is so large in the experiments for the $H=1$ configuration. On the other hand, according to this model, for large H the interaction is expected almost as soon as the second wave appears. However, these considerations did not take into account the dam-break motion in the mixed fluid; the combined influences may produce effects which require additional investigation.

The effect of the interaction between the wave and the head is indicated by the NS simulation of experiments of Amen & Maxworthy with small h_0/x_0 at $t \approx 6$ in figures 8 and 9 for the case with $H=2.7$, $h_0/x_0=0.33$. We observe that the main body of the intrusion becomes separated from the leading blob. The SW approximation, developed for a density-driven flow, is evidently not expected to be valid in these circumstances of transition to a wave-dominated flow. It is plausible that subsequently the leading portion of the intrusion will behave like the 'isolated propagating flow' phenomena investigated for descending thermals by Manasseh, Ching & Fernando (1998) (where other important references are given). The theoretical details of this transition and the evolution into the wave-dominated pattern require a separate investigation.

4. Cylindrical lock in a fully linearly stratified tank

The release from a cylindrical lock into a fully linearly stratified ambient ($l=H$) is relevant to the configuration studied experimentally by Wu (1969). Here $h_0=x_0$, $\mathscr{A}=\sqrt{H}$, and hence the reference velocity and time can be expressed as

$$U=\left(\frac{g'h_0}{H}\right)^{1/2}=\mathscr{N}h_0, \quad T=\mathscr{N}^{-1}. \tag{4.1}$$

The geometry of the lock introduces a sharp difference with the counterpart configurations of Amen & Maxworthy (1980) and de Rooij (1999) discussed in § 3.2. The contribution of this factor has not been properly considered in previous investigations and some confusion emerged. It is our objective to clarify this point. Another, and perhaps related, reason for ambiguity is the time scale of propagation. Following Wu, many investigations used the dimensionless time $\mathscr{N}t^*$ (which is based on the frequency of the internal waves in the ambient), but our SW formulation indicates that $\mathscr{N}t^*(h_0/x_0)$ (based on the propagation of the shallow-water waves in the intruding fluid) is more appropriate. Indeed, the initial motion is expected to be dominated by the propagation of the characteristics inside the body of mixed fluid, not by the waves in the ambient (see Ungarish 2005). These dimensionless times are identical for Wu's experimental configuration with $(h_0/x_0)=1$.

The speed of the waves in the ambient, the SW equations and boundary conditions for u are as for the rectangular case discussed in § 3.2. The motion starts, again, from rest. Up to this point the formulation is identical with that of the counterpart rectangular configuration discussed in § 3.2. Thus, (3.5)–(3.9) with $h_0/x_0=1$ can be applied. The change is in the initial condition of the interface, which is now

$$h(x)=(1-x^2)^{1/2} \quad (0\leqslant x\leqslant 1, t=0). \tag{4.2}$$

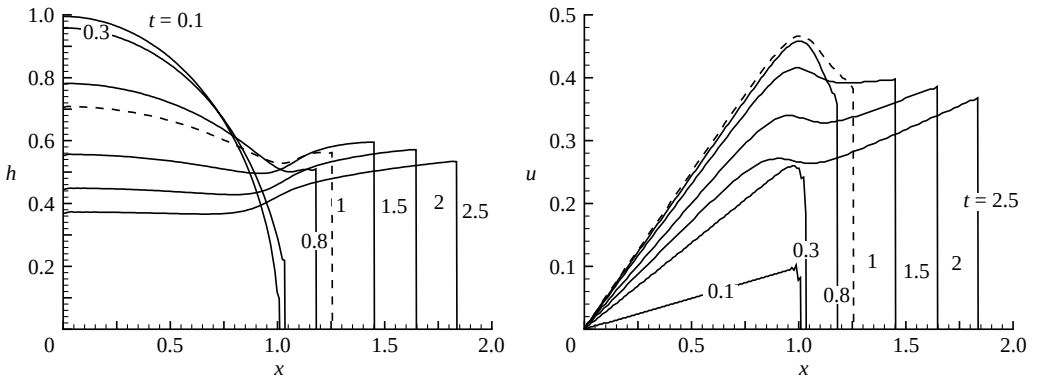

FIGURE 11. SW predictions for cylindrical lock, $H = 4$ (Wu's configuration): h and u profiles as a function of x at various t.

A simple analytical solution by the method of characteristics of the motion after release (like in the rectangular 'dam-break' problem which led to (3.10)) is not feasible. However, some useful approximations for the initial motion can be made. Since u and the (upward) displacement of the interface Δh are initially very small, we expand these variables in powers of t. Substitution in (3.6)–(3.7) yields the leading terms

$$u = xt, \tag{4.3}$$

$$\Delta h = \frac{1}{2}\frac{2x^2 - 1}{(1 - x^2)^{1/2}}t^2. \tag{4.4}$$

Note the stagnation point of the interface at $x = h = 1/\sqrt{2}$ where $\Delta h = 0$. The results indicate that immediately after release the intruding cylindrical body of fluid shrinks at the rear ($\Delta h < 0$) and thickens at the front (in remarkable contrast with a rectangular dam-break release). An inspection of the neglected terms (and comparisons with the numerical solution) indicates that these approximations are valid for $t \ll 1$ and $x < 1$. The (quite weak) singularity of Δh at $x = 1$ is relaxed by the development of a front of increasing height h_N that propagates forward to $x_N > 1$. The details cannot be obtained from this approximation, but continuity with (4.3) and characteristic balances indicate that $h_N \approx u_N \approx t$.

The finite-difference code for the SW equations handles the initial conditions of the cylindrical lock with no special difficulties (the numerical starting condition must be some small positive h_N, say 0.01, but the sensitivity to this condition in the subsequent solution, say, at $t > 0.05$, is very low). Comparisons with the finite-difference solution of the SW equations indicate that the previous approximate results capture well the features of the initial behaviour ($0 < t < 1$) and are in good quantitative agreement for $t < 0.5$.

In figure 11 we show, for the configuration of Wu, the SW profiles of the interface and velocity of the intrusion at various times. The shape is in fair agreement with the experimental observations sketched in figure 2(*b*) of Wu (1969). Contrary to common previous analytical models, the SW-modelled cylindrical-lock intrusion does not develop and preserve an elliptical shape. The behaviour of h and u in the rectangular-lock counterpart case is shown in figure 12. The SW predicted velocity of propagation u_N for Wu's configuration and the rectangular counterpart are shown in figure 13.

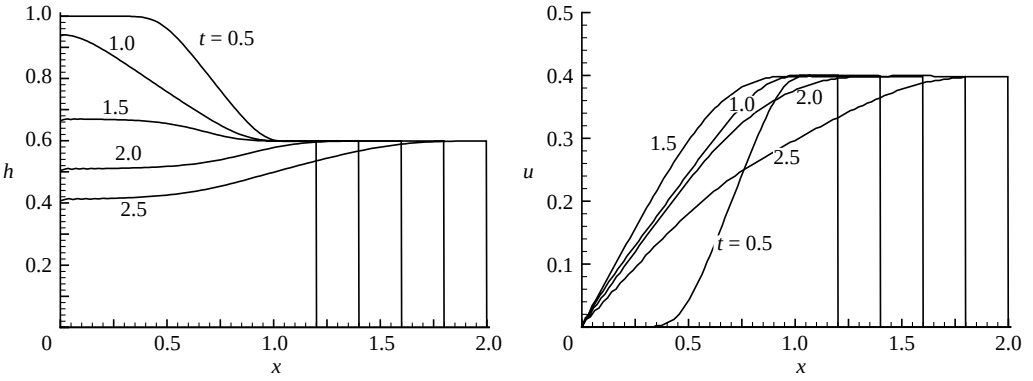

FIGURE 12. Rectangular-lock counterpart to figure 11: SW predictions of the h and u profiles as a function of x at various t.

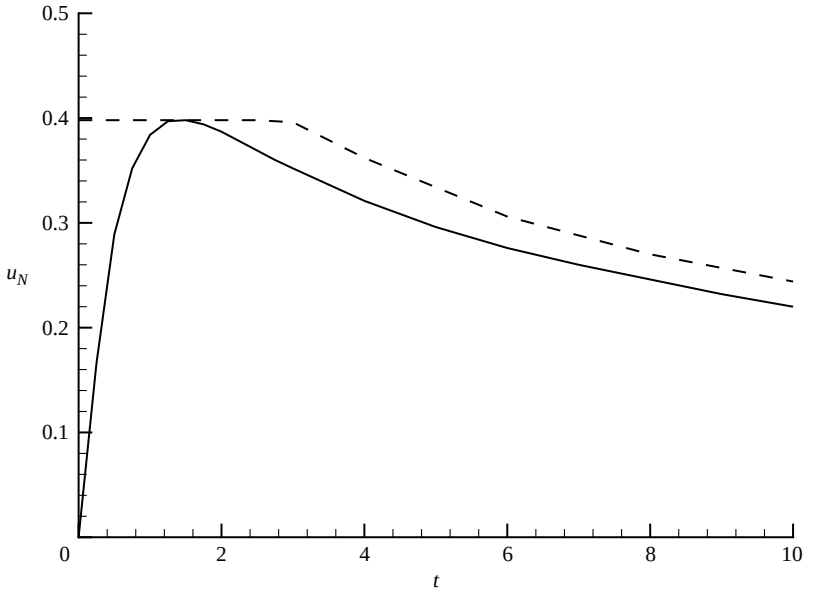

FIGURE 13. Velocity of propagation SW results: cylindrical lock (solid line) and rectangular-lock counterpart (dashed line). Here $H = 4$.

The main conclusion is that the initial behaviour in the cylindrical-lock case is different from that of the rectangular-lock counterpart. The reason for this effect is not the kinematic volume difference, but rather the internal dynamics and force distribution. In the hydrostatic state the mixed fluid in the cylindrical lock is subjected to a significant pressure gradient in the x-direction. Therefore, the removal of the lock induces accelerations in the whole body of fluid, and, from the start, a linear- with- x velocity profile develops, and the interface rises quickly in the domain $x > 1/\sqrt{2}$ and descends in the domain $x < 1/\sqrt{2}$. The overall initial trend is to straighten the interface to a horizontal position $h \approx 0.7$ at $t \approx 1$, while the nose almost develops the height and velocity of the slumping rectangular counterpart. However, the moving nose and the trailing region at $x > 1$ cannot maintain a constant-speed motion (as in the rectangular counterpart) because the forward-propagating characteristics that enter

this region are bound to carry time-dependent conditions. The SW approximation is expected to remain valid because the initial motion is governed by the hydrostatic pressure distribution, and subsequently the horizontal motion becomes dominant.

The SW velocity of propagation in Wu's configuration, see figure 13, has a clear two-stage pattern, of acceleration followed by deceleration, with a maximum at $t \approx 2$. The rectangular counterpart displays slumping with constant u_N and the deceleration starts later, at $t \approx 3.2$. The early transition to the deceleration phase renders the cylinder-lock configuration more prone to the self-similarity behaviour than the rectangular-lock counterpart. It is remarkable that, according to the SW results, the maximum u_N of the cylindrical lock release is equal to the constant slumping velocity of the rectangular-lock counterpart, i.e. the same H. This result can be explained via the balances on the characteristics c_+ which propagate from the initial stationary fluid in the lock. The special characteristic from $x = 0, t = 0$ in the cylindrical lock carries to the front the same information as all the characteristics released at $t = 0$ in the rectangular lock. Therefore the agreement in u_N is for a special point only.

We deduced that the SW propagation of an intrusion from a rectangular lock is always sub-critical, see figure 3. We now combine this result with the previous outcome concerning the maximum u_N attained in release from a cylindrical lock. We reach the conclusion that the propagation from a cylindrical lock release is also always sub-critical. This prediction of the SW theory is consistent with the observations of Wu.

Finally, we compare the present SW predictions of x_N as a function of t with the results of Wu (1969). The experiments were performed in a saline stratified tank with $H = 4$. The curve-fitted experimental data of propagation as a function of time produced the often-quoted formula

$$x_{N\,wu} = \begin{cases} 1 + (0.29 \pm 0.04)\,(\mathcal{N}t^*)^{1.08\pm0.05} & (0 \leqslant \mathcal{N}t^* \leqslant 2.5)\ \text{(the initial collapse stage)} \\ (1.03 \pm 0.05)\,(\mathcal{N}t^*)^{0.55\pm0.02} & (3 \leqslant \mathcal{N}t^* \leqslant 25)\ \text{(the principal collapse stage).} \end{cases} \tag{4.5}$$

This result has been considered as a prototype of the behaviour of an intrusion, but there is no reason why it should be valid for a configuration with a non-cylindrical lock and $H \neq 4$. The deviation bounds of the coefficients indicate a scatter (or error) of about $\pm 10\,\%$. The accuracy of the fit in the first stage is remarkably low, with deviations of up to 14 %. In our opinion, this is the result of the over-simplified fit rather than of experimental errors.

The comparison is shown in figure 14. The agreement between the SW solution and the experiment is very good. To be specific: the SW x_N is always larger than the value of (4.5), by at most 8 %, for $t \leqslant 25$. However, if we compare with the upper bound (due to scatter of data) of Wu's fit, $x_N = 1.08(\mathcal{N}t^*)^{0.57}$ for the second stage, we find that the SW results are smaller by about 2 %. We emphasize that the theory has been developed from first principles without any free adjustable parameters or use of specific empirical information taken from the experiment of Wu. This is in contrast with the previous models of Kao and Manins. The tendency of the theoretical SW prediction to overestimate the propagation can be attributed to the presence of small viscous and mixing dissipations in the real flow. The fact that the discrepancy is in the range of the experimental error provides, again, good support for the present SW formulation.

The SW model predicts that the transition from acceleration to deceleration occurs at $t = 2$. This is consistent with the transition at about $t = 2.5$ between the 'collapse

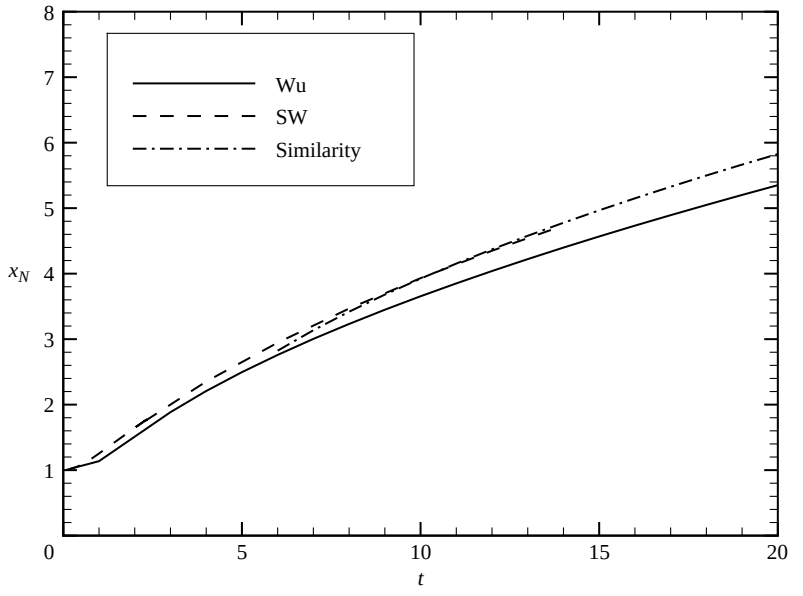

FIGURE 14. Results for Wu's configuration (cylindrical lock, $H = 4$) of x_N as a function of time: Wu's experimental fit, SW solution with initial conditions, and SW similarity result for large t with $\gamma = -1.7$ (see Appendix A). In the present case $t = \mathscr{N} t^*$.

stages' of Wu. The discrepancy (about 1 s in dimensional units) can be attributed to the lock removal interval (reported as 0.8 s). The very complex initial motion expected during this interval (at least) explains the low accuracy of Wu's simple curve-fit in the initial stage.

Wu's results are expected to provide a test case of the self-similarity solution discussed in Appendix A, because: (*a*) the recorded decaying-velocity regime starts quite early ($t = 3$) and covers a fairly long dimensionless time ($t = 25$); and (*b*) the intrusion is fairly deep ($h_N/H \approx 0.1$). The comparison, shown in figure 14, indicates that the predicted self-similarity behaviour is consistent with the experiments for $t > 10$ (more details are given in Appendix A).

5. Concluding remarks

The propagation of a symmetric intrusion (mixed fluid) of a given volume released at the neutral buoyancy level in a stratified ambient was considered. We introduced a new analysis, based on a one-layer shallow-water (SW) closed formulation, and backed by numerical solutions of the Navier–Stokes (NS) problem. Predictions were obtained for realistic geometries, and initial and boundary conditions. The theory does not rely on adjustable constants or predetermined shapes. Comparisons with published experimental data were performed.

Some essential issues have been clarified concerning the initial stages of propagation in stratified ambients (with both part-depth, $l < H$, and full-depth, $l = H$, density transition layers), in particular: the governing parameters and the influence of H and l on the velocity of propagation; similarities and differences between release from rectangular and cylindrical locks; the existence of a self-similarity solution and its connection with box-model approximations. All the theoretical results are consistent with the available experimental data.

The theory predicts that: (i) an intrusion released from a rectangular lock will propagate during the initial slumping stage with constant velocity, like a classical homogeneous gravity current; (ii) in contrast, the propagation after release from a cylindrical lock displays a clear acceleration–deceleration pattern; the maximum velocity is, remarkably, equal to the slumping u_N of a rectangular lock configuration with the same H. The deceleration process, which leads to a self-similar propagation, starts sooner than in the rectangular lock counterpart.

Prediction (i) is firmly supported by experimental and numerical results. The experiments of Faust & Plate (1984) provide a stringent test for u_N as a function of l in a full-depth lock configuration. The good agreement, within about 5 % over the full range of $0 \leqslant l \leqslant 1$, provides strong support for the SW theory. For the fully stratified ambient the SW slumping velocity is in agreement with the experiments within about 2–15 %. There seems to be no systematic discrepancy because the measurements are scattered about the theoretical curve (see figure 15). The SW slumping distance is shorter than the experimental and numerical values; this is a known deficiency of the one-layer model for $H < 2$.

Prediction (ii) is consistent with the experiments of Wu (1969). The predicted SW $x_N(t)$ agrees with the experimental curve-fit within the reported margin of accuracy of the latter.

For the developed motion, it was shown that propagation with $t^{1/2}$ is an exact similarity result of the SW equations in a very deep (say, $H/h_N > 10$) linearly stratified ambient. (For an intrusion in a shallow ambient the developed propagation corresponds to a larger power of t, approximately 3/5. For this case no exact solution of the SW equations was found.) Only the volume of the intrusion (not the shape of the lock) is relevant to the self-similar stage of motion. The experiments of Wu provide the only appropriate test case with (marginally) sufficiently deep intrusion and long time of unperturbed decaying motion. The experimental propagation is with the power 0.55 ± 0.02. We consider this an encouraging, but not clear-cut, agreement. In any case, the agreement with our result is better than with the homogeneous-current counterpart power 2/3.

The SW theory predicts that the velocity of the intrusion in a full-depth linearly stratified ambient is always sub-critical, for both rectangular and cylindrical locks, in agreement with the experimental observations. The excess over critical speed is about 10 % at $H = 1$ and increases with H.

The initial aspect ratio of the mixed fluid region (or of the lock), h_0/x_0, does not enter the SW formulation, and has little influence on the (properly scaled) velocity of propagation (before the interaction with the internal waves begins). However, we showed that the wavelength of the density-field perturbations is proportional to this parameter. Consequently, the length of 'unperturbed' propagation (i.e. before the interaction between the waves and the head of the intrusion stars) is proportional to h_0/x_0. An estimate for the position x_2 where the interaction begins was presented. This is consistent with the experimental data. A quantitative comparison was not attempted because a clear-cut definition of the interaction phenomena is lacking. This effect and the behaviour afterwards are left for future investigations.

The present SW formulation uses the one-layer model, which discards the motion of the ambient fluid. The model provides an excellent qualitative description of the initial motion, including accurate results for the velocity of propagation even for the $H = 1$ case. This good agreement (in many cases within the range of the experimental errors and/or of the deviations from the Boussinesq and inviscid idealizations) cannot be just coincidence. In our opinion, this is a clear-cut indication that the components

of the model, although not rigorously justified theoretically, capture well the essentials of the underlying physical mechanisms. This conclusion applies to the combination of: (i) the hyperbolic volume and momentum governing equation (2.14); (ii) the *Fr* correlation (2.19) (taken 'off the shelf' from the knowledge on the homogeneous gravity current); and (iii) the nose driving-force conjecture (2.17). All these components are necessary for the accurate description of the initial motion. It therefore makes sense to encourage the use and further development of these components. However, the one-layer assumption prevents the investigation of coupling effects between the upper and lower layers of fluid and is expected to be less accurate in the prediction of various details of the flow for configurations with H close to 1. In non-stratified circumstances the influence of the upper layer of fluid can be incorporated in a two-layer SW model. This coupling turns out to have a significant effect on some features (e.g. the slumping distance) for $H < 2$ configurations, as pointed out by Rottman & Simpson (1983), Klemp *et al.* (1994) and Ungarish & Zemach (2005). Unfortunately, the formulation and analysis of a corresponding two-layer model, with a second layer of stratified fluid, seems to be a formidable task. Theoretical considerations and the NS solutions indicate a very complex flow in the second layer which defies a straightforward extension of the homogeneous counterpart model. These topics are left for future work.

Overall, we think that good progress has been achieved from the motivating remark of Faust & Plate (1984): 'intrusions into a linearly stratified environment behave very differently from theoretical calculations', but there still are many topics that need investigation, both theoretically and experimentally. For example, three-dimensional, viscous and asymmetry effects, which were not incorporated in the present analysis, may play an important role in practical circumstances. Analytical and numerical studies of these effects are interesting topics for further investigations.

The state of experimental data prevents sharper conclusions about the performance of the present theory. Indeed, the information that can be obtained from the available experimental data is quite limited in both range and reliability. The available experiments cover only non-deep intrusions ($H \leqslant 2.5$ for rectangular lock release; and $H = 4$ for cylindrical lock). There are inconsistencies in the reported data, and almost no overlap between the parameter ranges considered by different parties. Most of these experiments were performed more than 20 year ago. We hope that the present study will provide the background, guidelines and the motivation for new and more complete sets of experiments.

Thanks to Professors T. Maxworthy, H. E. Huppert and J. Lister and Mrs T. Zemach for stimulating discussions and useful comments. The research was supported by the Fund for Promotion of Research at the Technion.

Appendix A. Similarity solution and box-model approximations

We consider a full-depth stratified ambient, $l = H$. The coefficient $\mathscr{A} = \sqrt{H}$, and the reference velocity and time are given by (3.4).

Self-similarity solutions play an important role in the SW analysis of gravity currents in a homogeneous ambient (see Grundy & Rottman 1985 and Slim & Huppert 2004 where other pertinent references are given). A natural question is whether and how this feature can be extended to the present problem.

We sought a self-similarity solution of the present SW equations of motion and the corresponding nose condition, for large values of t. When the intrusion is deep it is

justified to assume that $Fr = \text{const}$ ($= 1.19$ in our case, see (2.19)). For this case, we found that (3.6)–(3.8) are satisfied by

$$x_N(t) = K(t+\gamma)^{1/2}, \quad u = \dot{x}_N(t)y, \quad h = (b^2 + y^2)^{1/2}\dot{x}_N(t), \tag{A 1}$$

where $y = x/x_N(t)$ is the stretched horizontal coordinate, K and γ are constants,

$$b^2 = \frac{2}{Fr^2} - 1, \tag{A 2}$$

and the overdot means differentiation in time. We note that for the special value $Fr = \sqrt{2}$ (the value for the ideal deep homogeneous current developed by Benjamin 1968) the shape of h is linear with y. In any case, the present result for a linearly stratified ambient is very different from that of a current in a homogeneous ambient ($x_N \sim t^{2/3}$, $h \sim (C + y^2)\dot{x}_N^2(t)$), where C is a positive constant).

Conservation of the volume, $\mathscr{V}$, determines the value

$$K = (2\mathscr{V})^{1/2}\left[\int_0^1 (b^2 + y^2)^{1/2}\,\mathrm{d}y\right]^{-1/2}. \tag{A 3}$$

In the present scaling the values of $\mathscr{V}$ are 1 for the rectangular lock and $\pi/4$ for the cylindrical lock. We obtain $K = 1.537$ and 1.362, respectively.

The resulting flow has a 'virtual origin' because the physical $u = 0$ conditions and geometry of the lock at $t = 0$ cannot be imposed. The real time coordinate can be shifted by the parameter γ to achieve matching with the real initial slumping phase behaviour. This parameter turns out to be negative and, as expected, of order unity. Evidently, the applicability of the similarity solution to a real intrusion is only after the decay of the slumping stage, i.e. $t > 3$, at least. (This estimate is based on the time required for a backward–forward propagation of the characteristic in the initially motionless fluid, see (3.9), and is supported by detailed solution of the SW equations.)

The similarity solution is interesting from the academic point of view, as an exact solution to the governing PDE which describes the asymptotic $t \to \infty$ tendency of the system. Owing to its simplicity and rigour, it may be useful (*a*) for various tests of numerical schemes, and (*b*) as a basic state for perturbation techniques (e.g. Hogg, Ungarish & Huppert 2000; Harris, Hogg & Huppert 2002). We expect that the present result will facilitate the study of the transition to a wave-dominated motion. However, for practical applications the similarity solution is a quite weak predictive tool: it is restricted to deep intrusions at large times after release, and it is quite plausible that viscous, mixing and wave effects become influential in these circumstances. Moreover, the value of γ depends on the initial conditions and hence some additional assumptions, calculations or experiments must be involved in the use of (A 1).

The only available experimental test case for the similarity result is provided by Wu (1969). The other experimental results considered in our paper were not expected to display this behaviour because (*a*) the value of H is not sufficiently large, and (*b*) in rectangular-lock-release the transition to similarity is delayed by the constant-velocity slumping phase.

The comparison is displayed in figure 14 (§ 4). The details need some clarification. Our similarity result for a cylinder lock is $x_N(t) = 1.36(t+\gamma)^{1/2}$. We obtained $\gamma = -1.7$ from matching with the finite-difference SW computation. Wu's curve fit procedure ignored the 'virtual origin' constant γ and therefore obtained $x_N(t) = (1.03 \pm 0.05)t^{0.55\pm0.02}$. It still makes sense to compare the exponents, because, for $t > 10$ (say) the slope of x_N vs. t on a log-log plot (as used by Wu) will be little influenced by γ. The experimentally derived power of t is larger by 7–14 % than the theoretical 1/2.

A plausible explanation for this discrepancy is as follows: the $t^{1/2}$ propagation corresponds to a constant value of Fr, i.e. a very deep intrusion. The values of h_N/H in the experiment changed from about 0.15 to 0.10, and therefore Fr still increases during the propagation, see (2.19), and a more rapid than $t^{1/2}$ spread is expected. On the other hand, we recall that the similarity solution for a homogeneous ambient predicts the power of 2/3. Wu's result is clearly much closer to our prediction.

A simple box-model approximation can be obtained by the assumption that the similarity shape of the intrusion is a rectangle. Volume conservation $x_N(t)h_N(t) = \mathscr{V}$, the nose condition (3.8) and the correlation (2.19) yield a simple expression for $\mathrm{d}x_N/\mathrm{d}t$ whose integration provides

$$x_N(t) = \begin{cases} \left[\dfrac{5H^{1/3}}{6\sqrt{2}}\mathscr{V}^{2/3}\right]^{3/5}(t+C)^{3/5} & (0.075 \leqslant h_N/H \leqslant 1) \\ [1.19\sqrt{2}\mathscr{V}]^{1/2}(t+C)^{1/2} & (0 \leqslant h_N/H \leqslant 0.075, \text{ deep intrusion}). \end{cases} \tag{A 4}$$

The constant C is determined by an initial condition, such as $x_N = 1$ at $t = 0$, or by matching with a different result if available (as in Kao's theory discussed below). The speed of propagation decays with time and hence the initial (slumping) stage of motion (with constant or increasing speed) is not properly described by this approximation. On the other hand, we note that for a deep intrusion and large t there is perfect agreement with the similarity solution concerning the spread with $t^{1/2}$; this indicates that this behaviour is mainly a consequence of the nose condition and in particular the assumption that Fr is a constant. The models of Manins (1976) and Kao (1976), discussed below, also reflect this feature. On the other hand, we realize that an intrusion that is not deep ($h_N/H > 0.075$) is expected to propagate according to $t^{3/5}$. This theoretical indication of a larger than 1/2 power of t during the developed stage of propagation of an intrusion has not been presented before, to the best of our knowledge. However, this indication seems to be consistent with the power 0.55 ± 0.02 measured by Wu.

A comparison of the present SW results with the theoretical models of Manins (1976) and Kao (1976) is now in order. Neither of these two models is based on a solution of a system of governing equations, and both assume a predetermined shape of the intrusion in the principal (similarity) stage of motion: Manins an ellipse and Kao a rectangle. These shapes, and in particular the ellipse, are evidently in disagreement with the SW and NS solutions and with experiment (see figure 2(*b*) of Wu 1969). Moreover, these models attempted to reproduce Wu's observations and do not discern the influences of H, l, and of the initial shape of the lock on the behaviour of the intrusion. We note that Kao developed and used the nose condition $u_N = h_N$ (in our notation) which corresponds to a constant $Fr = \sqrt{2}$ in our equation (3.8). Using this condition, plus conservation of volume $\mathscr{V} = \pi/4$ and the assumption that the intrusion has a rectangular box shape, the propagation $x_N = 1.25(t+C)^{1/2}$ emerges, and this is essentially Kao's result for large t. The correspondence with the present box-model result for a deep intrusion, see (A 4), is evident. The value $C = -0.57$ has been determined by Kao via matching with an analytical approximation of Dugan *et al.* (1976) for the 'initial stage' ($t \leqslant 2.05$); the validity of this matching is debatable. Manins postulated a propagation nose condition based on an integral 'internal' Froude number, actually an adjustable parameter chosen to fit Wu's experiments; there is no clear-cut nose condition because the assumed elliptical shape imposes $h_N = 0$.

To summarize, Kao's description is more consistent with the present SW results than Manins'. Both Kao and Manins obtained the propagation $x_N = K(t+\gamma)^{1/2}$ for large t,

for the cylindrical lock release, by using some momentum-integral (or box-model) approximations. We showed here that this is a self-similar solution of the present SW governing equation, and a particular case of the approximations (A 4). These previous models can be considered a subset of approximate results of the present SW theory. They can now be dismissed (with due credit) because the present SW theory is based on a more rigorous formulation and has a much broader range of application and validity.

Appendix B. The Navier–Stokes simulations

We use a numerical finite-difference code which is a modified version of the software developed for the solution of a bottom gravity current in a channel, Ungarish & Huppert (2002). Symmetry with respect to the neutral-buoyancy level is not assumed, and hence the scalings of the variables and the position of $z = 0$ are different in the code described in this appendix from the SW formulation used in the main text.

The two-dimensional lock-release problem is simulated in a bounded rectangular domain, $0 < x < x_w, 0 < z < 2H$. The lock is in $0 \leqslant x \leqslant x_0, z_l(x) \leqslant z \leqslant z_u(x)$, where $\max(z_u - z_l) = 2h_0$ (here in dimensional form). For the rectangular lock z_l, z_u are constants, and the cylindrical lock is a semicircle with $h_0 = x_0$.

For numerical convenience we introduce the density function $\phi(\boldsymbol{r}, t)$ by

$$\rho(\boldsymbol{x}, t) = \rho_o[1 + \varepsilon\phi(\boldsymbol{x}, t)], \tag{B 1}$$

where

$$\varepsilon = \frac{\rho_b - \rho_o}{\rho_o}. \tag{B 2}$$

We expect $0 \leqslant \phi \leqslant 1$ in the domain of the ambient fluid, and $\phi = \phi_c < 1$ in the domain of the 'mixed' intruding fluid. In the linearly stratified symmetric case discussed here, $\phi_c = 0.5$.

We employ the following dimensionless balance equations:

1. conservation of volume

$$\nabla \cdot \boldsymbol{v} = 0; \tag{B 3}$$

2. momentum balance

$$\frac{\mathrm{D}\boldsymbol{v}}{\mathrm{D}t} = \frac{1}{1 + \varepsilon\phi}\left[-\nabla P - \phi\hat{z} + \frac{1}{Re}\nabla^2\boldsymbol{v}\right], \tag{B 4}$$

where P is the reduced pressure (defined in dimensional form by $P = p + \rho_o g z$);

3. density transport

$$\frac{\partial\phi}{\partial t} + \nabla \cdot (\boldsymbol{v}\phi) = \mathscr{D}\nabla^2\phi. \tag{B 5}$$

The relevant dimensionless parameters, in addition to ε, are the Reynolds number,

$$Re = \mathscr{U}\mathscr{L}/\nu, \tag{B 6}$$

and the dimensionless diffusion coefficient $\mathscr{D} = 1/Pe = 1/(\sigma Re)$, where Pe and σ are the Péclet and Schmidt numbers, respectively. Here $\mathscr{L}$ and $\mathscr{U}$ are the scaling length and velocity. In the numerical computations we employ $\mathscr{L} = x_0$ (the dimensional length of the lock) and $\mathscr{U} = (\varepsilon g x_0)^{1/2}$. The scale for time is $\mathscr{L}/\mathscr{U}$.

We are interested in flows with large values of Re, small ε and very small $\mathscr{D}$. Actually, the typical physical value of $\mathscr{D}$ is negligibly small (recall that $\sigma \gg 1$ for

saline solutions in water), but here a non-vanishing $\mathscr{D}$ is used in the solution of (B 5) as an artificial diffusion coefficient for numerical smoothing of the large density gradients of the moving interface.

The initial conditions at $t = 0$ are

$$\boldsymbol{v} = \boldsymbol{0} \quad (0 \leqslant x \leqslant x_{\mathrm{w}}, \quad 0 \leqslant z \leqslant 2H) \tag{B 7}$$

and

$$\phi = \begin{cases} \phi_c & (0 \leqslant x \leqslant 1, \quad z_l(x) \leqslant z \leqslant z_u(x)) \\ 1 - \dfrac{z}{2H} & \text{elsewhere.} \end{cases} \tag{B 8}$$

In the present runs z_l and z_u were symmetric about the midplane, and $\phi_c = 0.5$.

The boundary conditions for $t \geqslant 0$ are

$$\boldsymbol{v} = 0 \ \text{(on the bottom and sidewalls);} \tag{B 9}$$

$$w = 0, \quad \text{and no shear} \quad (z = 2H); \tag{B 10}$$

and

$$\hat{\boldsymbol{n}} \cdot \nabla\phi = 0 \quad \text{(on all boundaries),} \tag{B 11}$$

where $\hat{\boldsymbol{n}}$ is the unit normal vector.

These conditions contain some simplifications, in particular (B 10), which is the frictionless 'rigid lid' approximation for the free surface. In practical situations the free upper surface may have a height perturbation of magnitude ε during the flow. In addition, we assume that the lock is removed instantaneously and without any perturbation to the fluid, and that the flow is laminar.

The foregoing system of equations and boundary conditions was solved by a time-marching, finite-difference discretization method. The details are described in Hallworth *et al.* (2001) and will not be repeated here. The addition of stratification did not create any special numerical difficulties.

Briefly, the method is based on forward-time discretization of the velocity components, with implicit pressure terms. For each time step the continuity equation for the 'new' velocity field yields an elliptic equation for the 'new' pressure field.

The spatial discretization is performed on a staggered grid with il radial intervals and jl axial intervals. The variables P and ϕ are defined at mid-cell position denoted (i, j), u is defined at positions $(i \pm \frac{1}{2}, j)$ and w is defined at $(i, j \pm \frac{1}{2})$. Central spatial differences were used, with the exception of forward and backward differences for the advection terms in the density transport equation (B 5), which was treated by a MacCormack method to avoid spurious oscillations associated with the discontinuity of ϕ at the interface between the intrusion and the ambient. For this purpose we also used artificial diffusion, i.e. a larger value of $\mathscr{D}$ than dictated by molecular diffusion. This is justified by the fact that in the physical salt-water system used in the laboratory experiments, the value of the Schmidt number $\sigma = 700$, and hence the resulting diffusion layer during the time of propagation of the intrusion considered here is very thin, beyond the resolution of the feasible numerical grids. The truncation errors are second order in both time and space, and the grids and time steps were chosen with the aim of achieving accuracies of about 1 % in the velocity and ϕ fields. The major computational effort was invested in the solution of the discretized Poisson equation for $P_{i,j}$ at all grid points for each time step, by a bi-conjugate gradient method.

Typically, the simulations use $x_{\mathrm{w}} = 5$, grids of 200×200 intervals, and a time step 5×10^{-3}. Various tests and comparisons, performed with different grids and parameters, support the physical reliability of the results and indicate the numerical

H	h_0/x_0	u_N	u_{av}	u_{01}	u_{12}	u_{02}	Δ %	x_2	Run
1.00	1.00	0.28	0.26	0.26	0.27	0.26	1.6	15.7	167
1.00	1.00	0.28	0.24	0.23	0.24	0.24	1.4	14.5	170
1.28	1.10	0.30	0.24	0.23	0.24	0.24	2.8	5.6	111
1.32	0.59	0.30	0.25	0.25	0.25	0.25	1.7	4.4	103
1.32	1.05	0.30	0.21	0.20	0.21	0.21	2.5	4.9	110
1.39	1.00	0.31	0.21	0.21	0.21	0.21	0.3	4.4	105
1.47	0.56	0.31	0.38	0.39	0.37	0.38	2.9	8.3	96
2.27	0.33	0.35	0.27	0.28	0.27	0.27	2.6	2.6	116
2.27	0.33	0.35	0.29	0.30	0.29	0.29	1.7	2.5	117
1.28	1.10	0.30	0.21	0.18	0.23	0.21	13.3	4.7	113
1.32	1.05	0.30	0.19	0.17	0.20	0.19	9.7	5.5	107
1.32	1.05	0.30	0.17	0.15	0.19	0.18	12.1	4.2	108
1.39	1.00	0.31	0.20	0.21	0.18	0.19	8.6	4.2	106
1.32	1.05	0.30	0.20	0.18	0.21	0.20	8.4	5.1	112
1.39	0.58	0.31	0.26	0.24	0.28	0.27	10.4	5.2	101
1.47	0.56	0.31	0.35	0.38	0.33	0.34	8.7	7.1	97
1.47	0.56	0.31	0.36	0.39	0.34	0.35	8.7	6.5	98
1.79	0.29	0.33	0.45	0.49	0.42	0.44	9.6	5.1	86
2.50	0.31	0.36	0.25	0.29	0.22	0.24	15.6	2.2	114
2.50	0.31	0.36	0.29	0.34	0.24	0.29	17.6	2.1	115
1.28	0.59	0.30	0.17	0.23	0.13	0.15	34.6	3.8	104
1.56	0.32	0.32	0.32	0.41	0.22	0.33	30.6	5.5	78
1.67	0.29	0.32	0.45	0.34	0.55	0.45	23.3	2.5	82
1.79	0.28	0.33	0.42	0.30	0.51	0.45	29.3	2.6	75
1.72	0.27	0.33	0.25	0.33	0.20	0.21	33.8	6.3	69

TABLE 1. Velocity of propagation: the initial u_N predicted by the SW model, compared with values calculated from the measurements given in Table 1 of Amen & Maxworthy (1980). Δ is the maximum deviation from the average velocity, x_2 is the measured position where strong deceleration begins. The data of Runs 167 and 170 have been corrected for an apparent misprint in the original table (a shift of the decimal point).

accuracy of typically three significant decimal digits. We did not use the Boussinesq approximation, but in the cases of interest the typical $\varepsilon = 2 \times 10^{-2}$, and hence variations of this parameter by $\pm 20\,\%$ yielded insignificant changes in the numerical computations (the main influence of this variable is of course in the scaling quantities).

The numerical results reported in the paper were re-scaled according to the SW formulation, (2.11)–(2.12) and (3.4).

Appendix C. Comparisons with Amen and Maxworthy (1980)

Table 1 of that paper summarizes 25 runs with $2Hh_0 = 28\,\text{cm}$ (the height of the ambient in the tank), in the range $1 \leqslant H \leqslant 2.5$, $0.57 \leqslant \mathcal{N} \leqslant 1.78\ \text{s}^{-1}$, and various $0.29 \leqslant h_0/x_0 \leqslant 1.05$. The assumptions of Boussinesq and inviscid fluid were satisfied well (at least during the time intervals considered here). The typical distance and time of propagation are 50 cm and 20 s, respectively. If we assume plausible errors of $\pm 1\,\text{cm}$ and $\pm 1\,\text{s}$ (due to parallax, gate opening, diffusion) we obtain an estimate of the typical velocity measurement error as $\pm 7\,\%$. Since the experiments were not

repeated and the original records are not available it is very difficult to obtain a more accurate bound.

The table provides two recorded points (x_i, t_i), $i = 1, 2$ and the initial condition is $x_0 = 1$, $t_0 = 0$. We used this information to calculate, by finite differences, the velocities u_{jk} based on points j and k, and the average u_{av}.

Runs 167 and 170 were outside the reasonable range, and, following Faust & Plate (1984), we corrected the times given by multiplication by 10.

We present the processed data in table 1. We arranged the results in four groups, separated by horizontal lines, according to the magnitude of deviation from the average velocity. In the first group there are nine runs. Here the deviations from the constant-velocity propagation are typically 2 %. In the second group there are also nine runs, and the deviations are typically 10 %. The fluctuations of the velocity are not systematic: in some cases $u_{01} > u_{12}$, in other cases the opposite was obtained. Since the experimental error for this variable is estimated as 7 %, we claim that the first nine runs certainly reflect motion with constant velocity, while the next nine runs are fairly consistent with such a motion.

The position x_2 in all these experimental runs is also consistent with the expected slumping distance of a bottom gravity current and with the length of constant velocity observed in the experiments of Maxworthy *et al.* (2002). Therefore, in our opinion, these results support the theoretical prediction that a significant slumping phase with constant velocity appears.

The third group contains two experiments, both with $H = 2.5$ and $h_0/x_0 = 0.31$. Here the deviations from the constant-velocity pattern are about 17 %. However, there is also a difference of about 16 % between the average velocity of the two experiments for which we have no explanation. We therefore think that these results are inconclusive, and can be discarded from the analysis of the initial velocity pattern.

The forth group contains five experiments with $1.3 \leqslant H \leqslant 1.7$ and $0.3 \leqslant h_0/x_0 \leqslant 0.6$, and the deviations from the constant-velocity pattern are about 30 %. In experiments 78 and 104 we notice a strong drop in velocity from u_{01} to u_{12} (of more than 40 %). On the other hand, in runs 75 and 82 we see the opposite behaviour (an increase of more than 60 %). This is a bizarre inconsistency. In runs 75 and 82 large values of u_{12}, with no counterpart in other experiments, were obtained. Moreover, in run 69, performed with similar initial condition as runs 82 and 75, this velocity is by more than 60 % smaller. The inconsistencies in this group suggest the possibility that in these experiments the initial wave perturbation created by the opening of the gate influenced the results. In any case, the scatter in these experiments makes them inconclusive regarding the time-dependence of the velocity. We think that, again, these points can be discarded from the analysis of the initial velocity pattern.

We emphasize that our reservations about the data in the last groups is based on apparent internal inconsistencies, not on the deviation from the theoretical predictions. We do not suggest ignoring the fact that the theory disagrees with these experimental results. We only claim that, for the time being, there are reasons to discount the importance of these discrepancies. A clear-cut decision on this issue must be left to future experimental work.

In addition to the first nine experiments of table 1, clear-cut support for the constant slumping-velocity pattern in this configuration is provided by the results of de Rooij (1999) and of Maxworthy *et al.* (2002) (for a gravity current over a rigid boundary, in conditions quite similar to the upper half of an intrusion). A summary of these supportive results is presented in figure 15. We recall that the maximum u_N attained for release from a cylindrical lock is expected to be equal to the constant u_N for

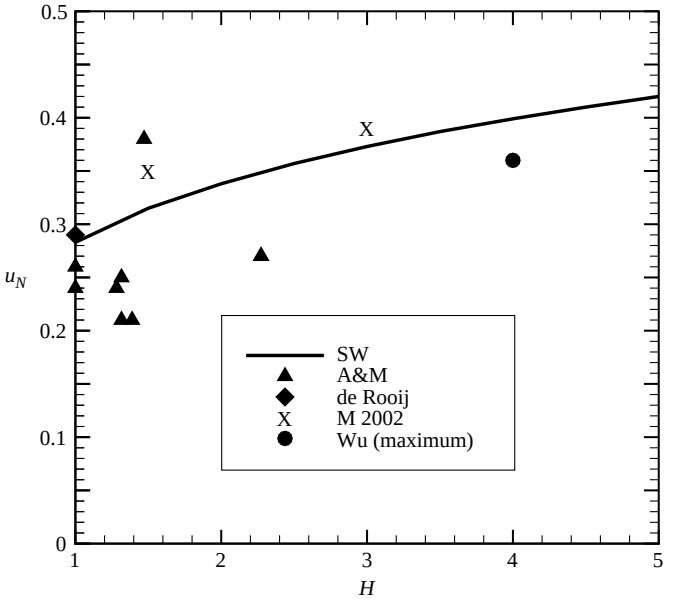

FIGURE 15. Slumping u_N as a functions of H in rectangular lock release, SW prediction and experimental results.

the rectangular-lock counterpart. Therefore, also shown in figure 15 is the maximum velocity derived from Wu's results. (We note that even here some uncertainties appear, see (4.5): at $t = 2.5$ the two curves give different results, 0.38 and 0.34; we used the average.) It is evident that the experiments cover only a very small domain of H, but overall various systems (i.e. stratifications, aspect ratios, tanks) are represented. It is encouraging that the experimental points are scattered about the theoretical line. This indicates that the model contains no major systematic error.

Values of x_2 from Amen & Maxworthy's experiments were compared in figure 10 with our estimate of the position where the first wave–nose interaction occurs. This is not a clear-cut effect and the comparison is mainly for a qualitative impression. We therefore applied a less stringent consistency test to the experimental data used for this figure, namely, a deviation of less than 100 % from the theoretical formula. This allowed the inclusion of 20 experimental points.

REFERENCES

AMEN, R. & MAXWORTHY, T. 1980 The gravitational collapse of a mixed region into a linearly stratified fluid. *J. Fluid Mech.* **96**, 65–80.

BAINES, P. G. 1995 *Topographic Effects in Stratified Flows.* Cambridge University Press.

BENJAMIN, T. B. 1967 Internal waves of permanent form in fluids of great depth. *J. Fluid Mech.* **29**, 559–592.

BENJAMIN, T. B. 1968 Gravity currents and related phenomena. *J. Fluid Mech.* **31**, 209–248.

BONNECAZE, R. T., HUPPERT, H. E. & LISTER, J. R. 1993 Particle-driven gravity currents. *J. Fluid Mech.* **250**, 339–369.

DUGAN, J. P., WARN-VARNAS, A. C. & PIACSEK, S. A. 1976 Numerical results for laminar region collapse in density stratified fluids. *Computers Fluids* **4**, 109–121.

FAUST, K. M. & PLATE, E. J. 1984 Experimental investigation of intrusive gravity currents entering stably stratified fluids. *J. Hydraulic Res.* **22**, 315–325.

Grundy, R. E. & Rottman, J. 1985 The approach to self-similarity of the solutions of the shallow-water equations representing gravity current releases. *J. Fluid Mech.* **156**, 39–53.

Hallworth, M. A., Huppert, H. E. & Ungarish, M. 2001 Axisymmetric gravity currents in a rotating system: experimental and numerical investigations. *J. Fluid Mech.* **447**, 1–29.

Harris, T., Hogg, A. J. & Huppert, H. E. 2002 Polydisperse particle-driven gravity currents. *J. Fluid Mech.* **472**, 333–371.

Hogg, A., Ungarish, M. & Huppert, H. E. 2000 Particle-driven gravity currents: asymptotic and box-model solutions. *Eur. J. Mech.* B **19**, 139–165.

Huppert, H. E. & Simpson, J. E. 1980 The slumping of gravity currents. *J. Fluid Mech.* **99**, 785–799.

Kao, T. W. 1976 Principal stage of wake collapse in a stratified fluid: Two-dimensional theory. *Phys. Fluids* **19**, 1071–1074.

Klemp, J. B., Rotunno, R. & Skamarock, W. C. 1994 On the dynamics of gravity currents in a channel. *J. Fluid Mech.* **269**, 169–198.

Manasseh, R., Ching, C.-Y. & Fernando, H. J. S. 1998 The transition from density-driven to wave-dominated isolated flows. *J. Fluid Mech.* **361**, 253–274.

Manins, P. C. 1976 Mixed region collapse in a stratified fluid. *J. Fluid Mech.* **77**, 177–183.

Maxworthy, T. 1980 On the formation of nonlinear internal waves from the gravitational collapse of mixed regions in two and three dimensions. *J. Fluid Mech.* **96**, 47–64.

Maxworthy, T. 1983 Experiments on solitary internal Kelvin waves. *J. Fluid Mech.* **128**, 365–383.

Maxworthy, T., Leilich, J., Simpson, J. E. & Meiburg, E. H. 2002 The propagation of gravity currents in a linearly stratified fluid. *J. Fluid Mech.* **453**, 371–394.

Morton, K. W. & Mayers, D. F. 1994 *Numerical Solutions of Partial Differential Equations.* Cambridge University Press.

Press, W. H., Teukolski, S. A., Vetterling, W. T. & Flannery, B. P. 1992 *Numerical Recipes in Fortran.* Cambridge University Press.

de Rooij, F. 1999 *Sedimenting particle-laden flows in confined geometries.* Ph D thesis, DAMTP, University of Cambridge.

de Rooij, F., Linden, P. F. & Dalziel, S. B. 1999 Saline and particle-driven interfacial intrusions. *J. Fluid Mech.* **389**, 303–334.

Rottman, J. & Simpson, J. E. 1983 Gravity currents produced by instantaneous release of a heavy fluid in a rectangular channel. *J. Fluid Mech.* **135**, 95–110.

Simpson, J. E. 1997 *Gravity currents in the Environment and the Laboratory*, 2nd Edn. Cambridge University Press.

Slim, A. C. & Huppert, H. E. 2004 Self-similar solutions of the axisymmetric shallow-water equations governing converging inviscid gravity currents. *J. Fluid Mech.* **506**, 331–355.

Ungarish, M. 2005 Dam-break release of a gravity current in a stratified ambient. *Eur. J. Mech.* B (in press).

Ungarish, M. & Huppert, H. E. 1998 The effects of rotation on axisymmetric particle-driven gravity currents. *J. Fluid Mech.* **362**, 17–51.

Ungarish, M. & Huppert, H. E. 2002 On gravity currents propagating at the base of a stratified ambient. *J. Fluid Mech.* **458**, 283–301.

Ungarish, M. & Huppert, H. E. 2004 On gravity currents propagating at the base of a stratified ambient: effects of geometrical constraints and rotation. *J. Fluid Mech.* **521**, 69–104.

Ungarish, M. & Zemach, T. 2005 On the slumping of high Reynolds number gravity currents in two-dimensional and axisymmetric configurations. *Eur. J. Mech.* B **24**, 71–90.

Wu, J. 1969 Mixed region collapse with internal wave generation in a density-stratified medium. *J. Fluid Mech.* **35**, 531–544.